Mechanism of Tripeptide Trimming of Amyloid β-Peptide 49 by γ-Secretase

Apurba Bhattarai[1], Sujan Devkota[2], Hung Nguyen Do[1], Jinan Wang[1], Sanjay Bhattarai[2], Michael S. Wolfe[2]* and Yinglong Miao[1]*

[1]Center for Computational Biology and Department of Molecular Biosciences,

[2]Department of Medicinal Chemistry, School of Pharmacy, University of Kansas, Lawrence, KS 66047, USA

* Corresponding emails: mswolfe@ku.edu, miao@ku.edu

Abstract

The membrane-embedded γ-secretase complex processively cleaves within the transmembrane domain of amyloid precursor protein (APP) to produce 37-to-43-residue amyloid β-peptides (Aβ) of Alzheimer's disease (AD). Despite its importance in pathogenesis, the mechanism of processive proteolysis by γ-secretase remains poorly understood. Here, mass spectrometry and western blotting were used to quantify the efficiency of tripeptide trimming of wildtype (WT) and familial AD (FAD) mutant Aβ49. In comparison to WT Aβ49, the efficiency of tripeptide trimming was similar for the I45F, A42T and V46F Aβ49 FAD mutants, but substantially diminished for the I45T and T48P mutants. In parallel with biochemical experiments, all-atom simulations using a novel Peptide Gaussian accelerated molecular dynamics (Pep-GaMD) method were applied to investigate tripeptide trimming of Aβ49 by γ-secretase. The starting structure was active γ-secretase bound to Aβ49 and APP intracellular domain (AICD), as generated from our previous study that captured activation of γ-secretase for the initial endoproteolytic cleavage of APP (Bhattarai *et al., ACS Cent Sci*, 2020, 6:969-983). Pep-GaMD simulations captured remarkable structural rearrangements of both the enzyme and substrate, in which hydrogen-bonded catalytic aspartates and water became poised for tripeptide trimming of Aβ49 to Aβ46. These structural changes required a positively charged N-terminus of endoproteolytic coproduct AICD, which could dissociate during conformational rearrangements of the protease and Aβ49. The simulation findings were highly consistent with biochemical experimental data. Taken together, our complementary biochemical experiments and Pep-GaMD simulations have enabled elucidation of the mechanism of tripeptide trimming of Aβ49 by γ-secretase.

Keywords: amyloid precursor protein (APP), proteolysis, Alzheimer's disease (AD), familial AD (FAD), Peptide Gaussian accelerated molecular dynamics (Pep-GaMD), mass spectrometry (MS).

Introduction

Alzheimer's disease (AD) contributes to more than 80% of all dementia cases [1]. Deaths related to AD in the United States increased by 89% between 2000 and 2014, and more than 6.2 million Americans are affected with AD in 2021 (www.alz.org). AD is characterized by deposition of longer amyloid β-peptides (Aβ) in the form of cerebral plaques. The amyloid β-protein precursor (APP) is successively processed by β-secretase and γ-secretase to produce Aβ peptides. β-Secretase first sheds the APP extracellular domain to produce transmembrane peptide C99, followed by processive proteolysis by γ-secretase to produce Aβ peptides of varying lengths [2]. Membrane-embedded γ-secretase is a multi-domain aspartyl protease with presenilin as the catalytic subunit. γ-Secretase is considered "the proteasome of the membrane", with more than 100 known substrates, including APP and the Notch family of cell-surface receptors [3-4]. The location of the proteolysis and the number of cleavages within the APP transmembrane domain by γ-secretase determines the length of final Aβ products and the likelihood of forming plaques.

Of the many transmembrane substrates, processive proteolysis of APP by γ-secretase is the most studied. γ-Secretase first carries out endoproteolytic (ε) cleavage of C99 peptide near the cytosolic end of the transmembrane domain, producing Aβ49 and Aβ48 peptides and their respective AICD co-products (AICD50-99 and AICD49-99, respectively)[5]. These initially formed long Aβ peptides are then cut generally every three residues from their C-termini to release tripeptide (and one tetrapeptide) co-products. The two general pathways of γ-secretase processive proteolysis are Aβ48→Aβ45→Aβ42→Aβ38 and Aβ49→Aβ46→Aβ43→Aβ40 [6-7], producing Aβ42 and Aβ40 as their dominant products, respectively. Among these two, the longer Aβ42 peptide is more prone to aggregate and forms plaques [8]. Moreover, early-onset familial AD (FAD) APP mutants can bias the enzyme to produce longer Aβ peptides that are pathological and cause

AD [9]. The trimming of APP substrate by γ-secretase enzyme is dictated by active site S1', S2' and S3'subpockets that respectively bind to P1', P2' and P3' substrate residues [10].

Critical gaps remain in understanding the mechanism of intramembrane processive proteolysis by γ-secretase. Recently reported cryo-EM structures of γ-secretase bound to Notch and APP substrates provided valuable insights into the structural basis of substrate recognition of the enzyme [11-12]. However, artificial structural constraints were included that could affect the enzyme-substrate interactions. Molecular dynamics (MD) simulations have proven useful in understanding the structural dynamics of γ-secretase, notably the enzyme-substrate interactions, including many previous studies[13-28]. Recently, we computationally restored the wildtype (WT) enzyme-substrate co-structure and applied all-atom simulations using the Gaussian accelerated molecular dynamics (GaMD) method to build the first dynamic model of γ-secretase activation[29]. GaMD is an enhanced sampling technique that works by adding a harmonic boost potential to smooth the potential energy surface and reduce system energy barriers [30]. Our GaMD simulations captured the extremely slow motions underlying enzyme activation, with the two catalytic aspartates and a coordinated water molecule poised for proteolysis of APP at the ε cleavage site. We showed that the I45F and T48P FAD mutations in APP enhanced the ε cleavage of the amide bond between Leu49-Val50 compared with the WT APP. In contrast, the M51F mutation in APP shifted the ε cleavage to the adjacent Thr48-Leu49 amide bond, changing the proteolysis from the Aβ49 to the Aβ48 pathway. Despite these advances, the detailed atomistic mechanism of processive proteolysis by γ-secretase remains elusive. This is consistent with γ-secretase being a well-known slow-acting enzyme (k_{cat} for APP ε proteolysis ~ 2-6 per hour) [31-32], making it difficult to capture the dynamic transitions comprising large energy barriers in MD simulations. Hence,

despite its importance in the pathogenesis of AD, the mechanism of processive proteolysis (tripeptide trimming) by γ-secretase remains poorly understood.

Here, we report the first dynamic model of tripeptide trimming of Aβ49 to Aβ46 (ζ cleavage) by γ-secretase. Extensive all-atom simulations using a novel Peptide GaMD (Pep-GaMD) method [33] captured the slow dynamic molecular transition from the ε to ζ proteolytic cleavage step. In Pep-GaMD, a boost potential is applied selectively to the essential potential energy of the peptide to effectively model its high flexibility and accelerate its dynamic motions [33]. In addition, another boost potential is applied on the protein and solvent to enhance conformational sampling of the protein and facilitate peptide binding. Pep-GaMD has been demonstrated on binding of model peptides to the SH3 protein domains. Independent 1-μs dual-boost Pep-GaMD simulations have captured repetitive peptide dissociation and binding events, which enable calculation of peptide binding thermodynamics and kinetics. The calculated binding free energies and kinetic rate constants agreed very well with the available experimental data [34].

In this study, we have combined biochemical experiments, including matrix-assisted laser desorption/ionization—time-of-flight) mass spectrometry (MALDI-TOF MS), liquid chromatography—tandem mass spectrometry (LC-MS/MS) and western blotting, with Pep-GaMD enhanced sampling simulations to elucidate the mechanism of tripeptide trimming of Aβ49 by γ-secretase. Our findings from Pep-GaMD simulations of WT and five FAD mutants (I45F, A42T, V46F, I45T and T48P) of Aβ49 bound to γ-secretase were highly consistent with quantitative biochemical analysis of their specific proteolytic products, providing important mechanistic insights into tripeptide trimming by the enzyme.

Results

Probing ζ cleavage of WT and FAD-mutant Aβ49 by γ-secretase in biochemical experiments.

To compare the ζ cleavage of the WT and FAD mutants of APP by γ-secretase, we performed *in vitro* cleavage assay experiments using purified γ-secretase and recombinant APP-based substrate C100-FLAG, which contained the C99 APP C-terminal fragment with an N-terminal start methionine and a C-terminal FLAG epitope tag [35]. Efficiency of the cleavage of substrate Aβ49 to products Aβ46 and tripeptide was calculated by measuring Aβ49 production and Aβ49 degradation. To quantify Aβ49 production by ε cleavage of APP substrate, levels of co-products AICD 50-99 were determined using a combination of matrix-assisted laser desorption/ionization time-of-flight mass spectrometry (MALDI-TOF MS) and quantitative western blotting.

First, AICD produced in the assay was immunoprecipitated with anti-FLAG antibodies and detected by MALDI-TOF MS (**Fig. 1A**). For the WT, A42T, V46F and I45T APP substrate, the signal intensities corresponding to AICD 49-99 and AICD 50-99 show higher level of AICD 49-99 than AICD 50-99. However, for mutants I45F and T48P APP substrate, signal intensities show higher level of AICD 50-99 than AICD 49-99. This suggests I45F and T48P favor production of Aβ49 rather than production of Aβ48 while A42T, V46F and I45T favor production of Aβ48 rather than production of Aβ49.

The same reaction mixtures were subjected to quantitative western blotting with anti-FLAG antibodies (**Fig. 1B**), where standards of known concentrations of C100-FLAG were also run to make a standard curve, plotting band intensity against concentration of FLAG-tagged C100. From this standard curve, the concentration of total AICD-FLAG product obtained in the enzyme reaction was quantified (**Fig. 1C**). Quantification of the total AICD revealed increased total AICD

production for V46F mutant substrate and decreased total AICD production for A42T, I45F, I45T, and T48P mutant substrates compared to AICD production for the WT. The concentration of AICD 50-99 was calculated using the total AICD level determined by quantitative western blot and the ratio of AICD 49-99 to AICD 50-99 determined from MALDI-TOF MS. (**Fig. 1D**). The calculated concentrations of AICD 50-99 thus provided the level of production of co-product Aβ49. Aβ49 production was slightly increased for I45F mutant, while for all other mutants A42T, V46F, I45T and T48P decreased Aβ49 production was observed compared to Aβ49 production of the WT.

To determine the degradation of Aβ49, we calculated and quantified trimming product tripeptide ITL. The mixtures from the cleavage assay were subjected to LC-MS/MS analysis to detect tripeptides. All substrate constructs studied produced ITL except for T48P mutant which produced IPL due to the replacement of T with P. For quantification of these tripeptides production, standard curves of each peptide were generated by plotting the concentration of synthetic peptide against the integrated areas of the three most abundant ion fragments from MS/MS (**Fig. S1**). The ITL and IPL peptide generated in the γ-secretase cleavage was monitored and quantified. (**Fig. 1E**). The quantification of the trimming product (ITL or IPL) or the Aβ49 degradation reveal decrease in Aβ49 degradation for A42T, V46F, I45T and T48P. For I45F, Aβ49 degradation is similar to that of the WT. Concentration of both Aβ49 production as well as Aβ49 degradation was used to calculate the percent efficiency (**Fig. 1F**). For all constructs, cleavage efficiency was close to 100% except that for two mutants I45T and T48P, the cleavage efficiencies decreased substantially to 35% and 34%, respectively.

We selected these particular FAD mutations in APP substrate based on their different effects on the Aβ49→Aβ46 trimming step in our recently reported study[31]. In that study, we examined the effects of 14 different FAD mutations in APP substrate on all proteolytic steps

carried out by γ-secretase. Moreover, we determined the Aβ42/40 ratios for these and other FAD mutations in APP substrate and found the relative effects of these mutations on this ratio compared to that seen with WT enzyme to be generally consistent with those reported from other groups[36-38]. To the best of our knowledge, the effects of the I45F, A42T, V46F, I45T and T48P FAD mutations of the substrate on the Aβ49→Aβ46 trimming step have not been reported by any other groups.

Activation of γ-secretase for tripeptide trimming of Aβ49 was captured in Pep-GaMD simulations.

In parallel with the biochemical experiments, Pep-GaMD simulations were carried out on the γ-secretase bound by the WT and the I45F, A42T, V46F, I45T and T48P mutants of Aβ49 **(Table 1)**. The active WT APP-bound γ-secretase was obtained from our previous study [29], and the amide bond between Aβ49 and AICD50-99 was cleaved as the new simulation starting structure **(Fig. S2,** see details in **Methods)**. We initially performed dual-boost GaMD simulations on the γ-secretase bound to Aβ49 with AICD50-99 removed. However, even after running ~6 μs GaMD simulations, we could not effectively sample conformational transitions of the system for ζ cleavage of Aβ49 to Aβ46 **(Fig. S3)**. The distance between the enzyme Asp257 catalytic residue and substrate Val46-Ile47 amide bond presented a computational challenge for conformational sampling, with apparently high energy barriers to overcome. To address the challenge, we applied our recently developed Pep-GaMD [33] method, which selectively boosts the essential potential energy of the peptide to effectively model the peptide flexibility and further improve sampling. We built four Pep-GaMD simulation systems with γ-secretase bound to Aβ49 in the presence of AICD50-99 and a system in the absence of AICD50-99 **(Fig. S4)**. The C-terminus of Aβ49 and

the N-terminus of AICD50-99 was either charged or neutral combined to form four different Pep-GaMD enzyme systems. Spontaneous activation of γ-secretase for ζ cleavage of Aβ49 was observed during 600 ns Pep-GaMD simulations with "charged C-terminal Aβ49 and charged N-terminal AICD50-99" **(Figs. S5** and **S6** and **Movie S1 and Table S2)**. The enzyme activation for ζ cleavage was characterized by coordinated hydrogen bonding between the enzyme Asp257 and carbonyl oxygen of substrate Val46. The catalytic aspartates were at a distance of ~7-8 Å between their Cγ atoms, which could accommodate a water molecule for nucleophilic attack of the carbonyl carbon of the scissile amide bond **(Fig S5)**. The water molecule formed hydrogen bonds with both catalytic aspartates and was at ~4 Å distance away from the carbonyl carbon of substrate Val46 residue. The activated γ-secretase conformation was well poised for cleavage of amide bond between Val46 and Ile47 for ζ cleavage of the Aβ49. In the γ-secretase bound to WT charged C-terminal Aβ49 and charged N-terminal AICD50-99system, we observed AICD50-99 dissociation in addition to enzyme activation for ζ cleavage **(Fig. S7 and Movie S2)**. The AICD50-99, initially located near the Aβ49, slowly moved downwards to the intracellular PS1 pocket and then dissociated completely from the enzyme. Meanwhile, the AICD50-99 transitioned from β-sheet to a loop/un-structured conformation during the Pep-GaMD simulations **(Fig. S7)**. Similarly, γ-secretase bound to "neutral C-terminal Aβ49 and charged N-terminal AICD50-99" was also observed to become activated for ζ cleavage of Aβ49. In comparison, the γ-secretase systems bound to "charged C-terminal Aβ49" (in the absence of AICD50-99), "charged C-terminal Aβ49 and neutral N-terminal AICD50-99", and "neutral C-terminal Aβ49 and neutral N-terminal AICD50-99" could not sample enzyme activation for ζ cleavage of Aβ49 (**Table S2**, **Fig. S6A-B, D** and **S8A-C**). This showed that the presence of charged N-terminal AICD50-99 was crucial for the enzyme activation for ζ cleavage of Aβ49. Therefore, systems for γ-secretase bound by charged

C-terminal Aβ49 and charged N-terminal AICD50-99 were set up for running Pep-GaMD simulations of the FAD mutants of Aβ49."

Free energy profiles were calculated from Pep-GaMD simulations to characterize the activation of γ-secretase for ζ cleavage of the Aβ49 substrate, for which the distance between the enzyme catalytic aspartates and the distance between the enzyme protonated Asp257 and substrate residue Val46 were selected as reaction coordinates **(Fig. 1G-1L, S6 and S9 and Table S2)**. In the WT Aβ49, three low-energy conformational states were identified from the free energy profile, including "Final", "Intermediate" and "Initial" **(Figs. 1G, S6C and S10 and Table S2)**. In the "Final" conformational state, the aspartates were ~7-8 Å apart to accommodate the water molecule in between. The substrate Val46 maintained a distance of ~3 Å from the active site Asp257 to form hydrogen bond in the Final active state. In the "Initial" state, the substrate Val46 was distant (~8-9 Å) from the active site Asp257, while the inter-aspartate distance was ~6-7 Å. The "Initial" state represented the active state for the ε cleavage of APP. In the "Intermediate" state, the aspartates remained ~6-7 Å apart, while the Aβ49 peptide (carbonyl oxygen of Val46) was at a distance of ~6 Å from the protonated Asp257 **(Fig. 1G)**.

In the I45F mutant system, two low-energy conformational states, "Initial" and "Final", were identified from the free energy profile of Pep-GaMD simulations **(Figs. 1H, S11A and S12A and Movie S3)**. Two out of three Pep-GaMD simulations could capture the activation process, as the Asp257 could form stable hydrogen bond with Val46 as reflected in the distance time course plot (**Fig. S11A**). The "Final" state in the free energy profile represented the active conformation of the enzyme for ζ cleavage of the scissile amide bond between Val46 and Ile47 APP residues. In the "Final" conformational state, the two catalytic aspartates were ~7-8 Å apart, and APP Val46 was ~3 Å distance away from the protonated aspartate. In the "Initial" state, the substrate Val46

was further away from the catalytic aspartate (~6-7 Å), and the aspartates were ~7-8 Å distance away from each other **(Fig. 1H)**.

In the A42T mutant APP system, four low-energy conformational states were identified from the free energy profile **(Figs. 1I, S11B and S12B and Movie S4)**. Mutation of Ala42 to Thr42 caused the enzyme-substrate complex to sample a larger conformational space. In addition to the "Initial" and "Final" states, two new "Inhibited-1" and "Inactive" conformational states were identified for the A42T mutant system. The catalytic aspartates were ~4-5 Å (too close) apart in the "Inhibited-1" state and 13 Å away (too far) in the "Inactive" state. In the "Inhibited" state, the catalytic aspartates could not accommodate a water molecule between them and hence was inhibited from proteolytic activation. APP Val46 was ~4-5 Å from the protonated Asp257 in this "Inhibited-1" state. In the "Inactive" state, the aspartates were ~13 Å apart and thus too far to form the dual hydrogen bonds with the water in between them, even though the Asp257 could form a hydrogen bond with the Val46 carbonyl oxygen. This hindered activation required for ζ cleavage.

In the V46F mutant system, two low-energy conformational states were identified, including "Inhibited-2" and "Final" **(Figs. 1J, S11C and S12C and Movie S5)**. Like other γ-secretase systems, the "Final" state corresponded to the active conformation of the enzyme poised for ζ cleavage of Aβ49. Moreover, the "Inhibited-2" state had the two aspartates at proximity (~4-5 Å) between the Cγ atoms and unable to accommodate a water molecule in between for enzyme activation. APP substrate was ~10 Å away from active site Asp257 in the "Inhibited-2" state.

Furthermore, Pep-GaMD simulations were carried out on I45T and T48P mutant Aβ49-bound γ-secretase **(Figs. 1K-1L, S11D-S11E and S12D-S12E)**. Both of these mutant systems were not able to activate the enzyme for ζ cleavage, being consistent with the experimental results where the ζ cleavage efficiency dropped to about one third compared to that of the WT. In the Pep-GaMD

free energy profile of the I45T mutant system, only one "Intermediate" low-energy conformational state was identified. This "Intermediate" state was the same low-energy conformation as the one in the WT system. For the T48P system, the hydrogen bond between APP Val46 and the protonated Asp257 was formed for a certain time in one of the three Pep-GaMD production simulations **(Fig. S11E)**. However, in the free energy profile, we could identify two low-energy conformational states, including "Initial" and "Inhibited-1", but not the "Final" active state **(Fig. 1L)**. The "Inhibited-1" state resembled the one identified in the A42T mutant system. The "Initial" conformational state was the same as the one identified in the WT, I45F and A42T systems. These Pep-GaMD simulation findings were consistent with the biochemical experiments, verifying the I45T and T48P systems as negative controls.

Conformational changes in activation of γ-secretase for tripeptide trimming of Aβ49

We calculated root mean square fluctuations (RMSFs) of γ-secretase bound by the WT and FAD-mutant APP from Pep-GaMD simulations **(Fig. S13 and Movie S6)**. In the WT Aβ49-bound γ-secretase, the TM2, TM6, TM6a and C-terminus of TM9 helix were flexible in the catalytic PS1 subunit. The Pen-2 subunit exhibited high fluctuations with ~ 3 Å RMSF. Helices a1, a2, a5, a12, a17, and TM domain of nicastrin were also flexible during the Pep-GaMD simulations. Structural clustering was performed on Pep-GaMD snapshots of the system using hierarchical agglomerative algorithm in CPPTRAJ [39] (see **Methods**). The top-ranked cluster was selected as the representative "Final" active conformation for the ζ cleavage of Aβ49. The starting structure from ε cleavage of APP was obtained as the "Initial" active conformation. The catalytic PS1 of the "Final" conformation was compared to that of the "Initial" conformation in **Fig. 2A**. Relative to the "Initial" conformation, the substrate helical domain tilted by ~50 degrees in the "Final"

conformation **(Figs. 2A** and **2B)**. Residue Leu49 in the substrate C-terminus moved downwards by ~5 Å **(Figs. 2B**, **4A** and **S14)**. The last residue in a helical conformation in the "Final" state of Aβ49 was Thr43 whereas it was Ile45 in the "Initial" state. In transition from the "Initial to the "Final" conformational state, two substrate residues, Val44 and Ile45 unwound their helical conformation and changed to a turn/loop conformation. Residues Thr43 and Ile45 were in similar positions in the "Initial" and "Final" active conformations relative to the membrane perpendicular axis (**Fig. S14**). In comparison, the substrate C-terminal Leu49 moved downwards by ~5 Å while straightening the C-terminal loop **(Figs. 2B and S14B)**.

At the enzyme active site, the catalytic Asp385 did not have significant movement during the adjustments for substrate peptide trimming (**Fig. 2C**). In comparison, the protonated catalytic Asp257 moved by ~3 Å towards the substrate. Asp257 moved forward to form a hydrogen bond with the carbonyl oxygen of the scissile amide bond between the substrate residues Val46 and Ile47. Similarly, TM3 moved outwards by ~2 Å **(Fig. 2D)**, and TM6a moved downwards by ~2 Å **(Fig. 2E)**. Flexibility in these helices involved important FAD mutation sites including Tyr154, His163, Ala164, Leu166, Trp165, Ser169, Ile168, Tyr256, Ala260, Leu262, Cys263, Pro264, Pro267, Arg269, Val272 and Leu271 (www.alzforum.org). Trp165 and His163 from TM3 and Arg269 from TM6a showed significant movements in their side chains. With a major part of C-terminus of APP absent (as AICD dissociates, see next section) the β2 loop at N-terminus of TM7 moved away from the APP by ~5 Å in the Final state as compared to the Initial state **(Fig. 2F)**. FAD mutation residues in the β2-TM7 region including Arg377, G378, L383 and G384 showed flexibility in the simulations. In particular, residue Arg377 reoriented its side chain in the "Final" conformational state.

Changes in secondary structures of the WT and FAD-mutant Aβ49 during tripeptide trimming

Secondary structures of the WT and FAD-mutant Aβ49 bound to γ-secretase were recorded during the Pep-GaMD simulations and plotted in **Figs. 3 and S15**. Changes in secondary structures of Aβ49 during ζ cleavage were compared to that of APP substrate ("Initial" active conformation) during ε cleavage from our previous study [29] **(Fig. S16)**. Unwinding of the helix C-terminus in Aβ49 during ζ cleavage was observed in the secondary structure plot. During the ε cleavage, the C-terminus of the WT APP substrate could maintain helical conformation up to Ile45/Val46 **(Fig. S16)**. In comparison, WT Aβ49 was helical up to Thr43 in the C-terminal region **(Figs. 3A and 2B)**. About 2-3 residues unwound near the ζ cleavage site to expose the scissile amide bond between Val46 and Ile47 to the catalytic aspartates and the coordinated water for activation. A new helix was formed for residues Ser26 to Ala30 in the Aβ49 during the transition from ε to ζ cleavage in the WT system **(Figs. 3A and S17)**. With the 50° tilt of Aβ49 peptide in the space between TM2 and TM3, the N-terminus is exposed to the hydrophobic lipid bilayer **(Fig. S17)**. This helped the N-terminal loop to transition to a α-helical conformation. The effects of the mutations on the new helical conformation is mentioned and explained in the next paragraph. A turn/unstructured conformation at residues Ala30-Ile31 separated these two helices. In addition, the N-terminus of Aβ49 lost its interactions with the hydrophobic loop 1 (HL1) because of the tilting away from this loop.

Similarly, secondary structural changes were recorded for the I45F, A42T and V46F Aβ49 mutant systems **(Figs. 3B-3D and S15)**. Like the WT, the I45F and A42T Aβ49 mutants maintained a helical conformation up to Thr43 at the N-terminus during the Pep-GaMD simulations. C-terminal residues after the Thr43, which included the ζ cleavage site bond between Val46 and

Ile47, were observed mostly in a turn/unstructured conformation. This allowed the catalytic aspartates and water to approach the scissile amide bond for forming coordinated hydrogen bonds required for this cleavage. Likewise, bands of new helix formation were observed in the secondary structure plots from Asn27 to Ile31 and from Asp23 to Lys28 for I45F- and A42T-mutant Aβ49 systems, respectively **(Fig. 3B and 3C)**. The new helix formed was due to its exposure to the hydrophobic lipid membrane. V46F Aβ49 was observed to be the most dynamic in terms of secondary structure changes **(Fig. 3D)**. A band of helix was observed between Gly29 to Thr43, with a turn conformation formed between Leu34 – Val36. Thr43 to Ile47 transitioned between helix and turn conformations during the Pep-GaMD simulations of the V46F Aβ49. Like the WT and other mutant systems, new N-terminal helix formation was observed at residues Phe20 to Gly25 in the V46F mutant APP **(Fig. 3D)**. The hydrophobic lipid environment helped these residues transition from turn to a helical conformation in the V46F mutant APP.

Active-site subpockets formed in γ-secretase for tripeptide trimming.

The "Final" active conformational state of Aβ49-bound γ-secretase was further analyzed for the P1', P2' and P3' substrate residues at the ζ cleavage active site and the respective S1', S2' and S3' subpockets in which they reside [10]. The S1' subpocket accommodating the P1' residue in the WT Aβ49 was formed by residues from PS1 TM6a helix, β1 loop, TM3 helix and TM7 N-terminal region **(Figs. 2 and 4A)**. The residues that formed the subpockets are listed in **Table S1**. The S2' subpocket occupied by the P2' substrate residue consisted of residues from PS1 TM6 helix, TM6a helix, PAL motif of TM9 helix, β1 and β2 loop region. Moreover, the S3' subpocket accommodating the P3' residue was formed by residues from PS1 TM6 helix, TM6a helix and β1

loop. In reference to Aβ49, S1' and S3' pockets were located on the same side (TM6a and TM3 helices) whereas the S2' pocket was located on the opposite side (TM6 and TM9 helices).

Similarly, the "Final" active conformational states of the I45F and A42T mutant Aβ49-bound γ-secretase systems had the same subpockets formed at the active site during the ζ cleavage as that of the WT system **(Fig. 4B-4C and Table S1)**. In the I45F and A42T "Final" active conformation, the S1' and S3' subpockets occupied by the respective P1' and P3' substrate residues consisted of residues from PS1 TM6 helix, TM6a helix, TM7 helix, β1 and β2 loop region. In comparison, the S2' subpocket was located on the opposite side of Aβ49 and consisted of residues from PS1 TM6 helix, TM6a helix, PAL motif of TM9 helix, β1 and β2 loop. Furthermore, in the V46F "Final" active conformation, the locations of the S1' and S2' subpockets accommodating P1' and P2' Aβ49 substrate residues, respectively, were different as compared to that of the WT system **(Fig. 4C-D)**. The S1' pocket occupied by the P1' residue of Aβ49 consisted of residues from TM6 helix, TM6a helix and TM2 helix **(Table S1)**. The S2' subpocket occupied by the P2' residue of the V46F mutant in the "Final" active state was the same as the S1' subpocket in the "Final" active state of the WT, I45F and A42T systems **(Fig. 4C-D)**. Moreover, the S3' subpocket accommodating the P3' substrate residue in the V46F mutant was the same as the one of the WT, I45F and A42T systems (**Fig. 4E**).

Discussion

Current AD treatments ease symptoms, but none has been clearly demonstrated to slow or halt disease progression. While the molecular cause of AD remains poorly understood, the hallmark pathological criteria for AD diagnosis is the deposition of amyloid-β (Aβ) plaques in the brain [40]. Aβ peptides are products of processive proteolysis by γ-secretase. Dominant missense mutations

in the substrate (APP) and the enzyme (presenilin component of γ-secretase) cause early-onset FAD, and these mutations result in deficient carboxypeptidase trimming of initially formed long Aβ peptides to shorter secreted forms [31, 41-42]. Yet the mechanism of processive proteolysis of APP by γ-secretase is unknown. Recent reports of cryo-EM structures of γ-secretase bound to APP and Notch substrates as well as to γ-secretase inhibitors and modulators revealed details of the structural basis of substrate recognition as well as enzyme inhibition and modulation [11-12, 43]. Regardless, static conformations of the enzyme cannot explain the underlying mechanism of enzyme activation and substrate processing. Essentially nothing is known about the dynamic mechanism of processive proteolysis by γ-secretase.

It would require quantum mechanics/molecular mechanics (QM/MM) calculations to fully understand the catalytic mechanism of proteolysis by γ-secretase. The catalytic step is likely the rate-limiting step of the enzyme proteolysis, being slower than the substrate-enzyme interaction dynamics. Nevertheless, the latter (dynamic motions of the substrate-enzyme interaction) has been suggested to take place over minutes[32]. This is still considered as slow dynamics and extremely long timescales that is way beyond the reach of *state-of-the-art* conventional MD simulations, but amenable to enhanced sampling simulations. We initially performed ~6 μs regular dual-boost GaMD simulations but could not sample stable enzyme-substrate hydrogen bond that characterizes system conformation for ζ cleavage of Aβ49 **(Figure S3)**. Then we turned to our recently developed Pep-GaMD method, which selectively boosts the essential potential energy of the peptides. Pep-GaMD has been demonstrated to greatly accelerate protein-peptide binding simulations by orders of magnitude[33]. Compared with previous GaMD, Pep-GaMD is a more powerful method that can be applied for further improved enhanced sampling of protein-peptide interactions. The new Pep-GaMD simulations allowed us to capture the ζ cleavage activation in

600 ns. In this context, novel Pep-GaMD simulations have, *for the first time*, captured slow dynamic conformational transitions in both the enzyme and substrate for tripeptide trimming of the wildtype and FAD mutants of Aβ49, being consistent with MS and western blotting biochemical experiments.

Here, we have applied the combination of novel Pep-GaMD enhanced sampling simulations and biochemical experiments to address the issue. Different systems of γ-secretase bound by the WT and FAD-mutant Aβ49 substrates were investigated to understand tripeptide trimming, ζ cleavage **(Fig. 5)**. Five γ-secretase systems—bound to the WT, I45F, A42T and V46F charged C-terminal Aβ49 in presence charged N-terminal AICD50-99 and bound to WT neutral C-terminal Aβ49 and charged N-terminal AICD50-99— underwent activation for ζ cleavage during 600 ns Pep-GaMD simulations **(Fig. 5B)**. This was consistent with biochemical experiments, as these mutant systems showed similar efficiencies for the Aβ49 to Aβ46 proteolytic step (ζ cleavage). In comparison, γ-secretase bound by I45T and T48P Aβ49 showed little or no sample activation **(Fig. 5C)**. Furthermore, Aβ49-bound γ-secretase in the absence of AICD50-99 was not able to sample the "Final" active state for ζ cleavage of the substrate **(Fig. S8A)**, similarly for γ-secretase bound to WT charged C-terminal Aβ49 and neutral N-terminal AICD50-99 and γ-secretase bound to WT neutral C-terminal Aβ49 and neutral N-terminal AICD50-99 **(Fig. S8B-S8C)**. This highlighted the importance of AICD50-99 and its N-terminal charge in facilitating processive proteolysis by γ-secretase. Following ε cleavage, both the C-terminus of Aβ49 and N-terminus of AICD50-99 at the active site could be exposed to water molecules and thus charged at physiological pH 7 (as carboxylate and ammonium, respectively). The charged state likely aided movement toward the polar aqueous environment and away from the hydrophobic transmembrane interior of the PS1 active site. Indeed, the AICD50-99 with charged N-terminus could dissociate

from PS1 in the Pep-GaMD simulations that helped prepare for the next cleavage during processive proteolysis by γ-secretase.

During ζ cleavage activation, two residues unwound from the C-terminus of the Aβ49 helix, changing to a turn conformation **(Fig. 5B)**. This was observed in the time courses of the substrate secondary structures as well. Unlike the helical conformation, the loop/turn conformation facilitated exposure of the scissile amide bond to the catalytic aspartates and the coordinated water molecule. In parallel, positions of the Thr43 and Ile45 residues in the "Initial" and "Final" states relative to the membrane were similar, whereas the C-terminal residue Leu49 moved downwards by ~5 Å. Moreover, the helical domain of Aβ49 tilted by ~50 degrees **(Fig. 5B)**. Thus, tilting of the helical domain and unwinding of C-terminal helix in the substrate apparently facilitated the proteolytic progression from ε to ζ cleavage by γ-secretase. Helix unwinding was accompanied by straightening of the C-terminal loop/turn and downward movement of the terminal residue Leu49. Similarly, the β-sheet conformation between the APP C-terminus and the β1 loop was broken as ε cleavage product AICD50-99 dissociates. This caused the β1 loop to move away from the APP C-terminus by ~5 Å. This region has been suggested to be important for substrate recognition and proteolytic processing [12]. Similarly, γ-secretase inhibitors (GSIs) and transition state analogs (TSAs) bind to this region [43]. The present study also shows an important role of this region in activation of γ-secretase for ζ cleavage of Aβ49.

Relevant to this study, Hitzenberger et. al.[13] performed restraint MD simulations to produce γ-secretase complex structure bound to the Aβ49, Aβ46 and Aβ43 peptides. Simulations on these complexes showed that both helix unwinding and sliding of active site aspartates towards the scissile amide bond are responsible for peptide repositioning during substrate processing by γ-secretase. During repositioning of the Aβ peptides, the N-terminus was anchored to maintain its

interaction with PS1 subunit. However, these enzyme-substrate model complexes were generated by combining apo γ-secretase missing the Nicastrin subunit and C99 peptide using restrained MD. AICD50-99 peptide was not included in the γ-secretase study and charges on the terminal ends of the Aβ49 and AICD50-99 peptide were not considered. In comparison, our model was based on the holo enzyme activated for ε cleavage from our previous study[29] generated using the APP bound γ-secretase cryo-EM structure. To the best of our knowledge, we are unaware of previous studies on the molecular dynamics of tripeptide trimming, in particular trimming of Aβ49 to Aβ46, by the γ-secretase complex.

Pep-GaMD captured the enzyme activation for ζ cleavage for γ-secretase systems bound to WT and three FAD-mutant (I45F, A42T and V46F) APP substrates. The low-energy "Final" active conformation was identified in the Pep-GaMD free energy profiles of all these systems. However, the PMF profiles representing each enzyme system was different in terms of distinct low-energy states and the conformational space sampled by the enzyme during ζ cleavage. The I45F and V46F mutant systems sampled two low-energy conformations with the I45F system being the least conformationally dynamic **(Fig. 1H, J)**. Three and four low-energy states were identified from free energy profiles of the WT and the A42T mutant systems, respectively, with the A42T mutant system being more dynamic **(Fig. 1G, I)**. Each system had its own set of conformations and a distinct activation pathway. This suggested that the enzyme is remarkably dynamic, consistent with its ability to cleave over 100 different substrates[44].

In the "Final" active state of γ-secretase poised for the ζ cleavage, subpockets were formed in the active site that were different from that formed for the ε cleavage **(Fig. 4 and S20)**. This finding was consistent with the observation that the C-terminus of Aβ49 during ζ cleavage did not form a β-sheet conformation with the PS1 TM6a β2 region, instead adopting a loop conformation

(Fig. 2F). The locations of the active site subpockets formed for ζ cleavage were compared to those formed for ε cleavage **(Fig. S20)**. Moreover, the locations of S1', S2' and S3' subpockets formed for ζ cleavage were the same for different γ-secretase systems bound to the WT and mutant Aβ49 except for the V46F mutant system. The S2' subpocket accommodating the T48 P2' residue formed for ζ cleavage was the same as the S1' subpocket accommodating the V50 P1' subpocket formed for ε cleavage. In contrast, the ζ cleavage S3' subpocket for the L49 P3' residue was the same as the ε cleavage S3' subpocket for the L52 P3' residue. The S1' subpocket for the I47 P1' residue for ζ cleavage and the S2' subpocket for the M51 P2' residue for ε cleavage had their own unique location in their respective Final active states. Regardless, S1'/S3' and S2' subpockets were located on opposite sides of the substrate in both of the "Initial" and "Final" active states.

During 600 ns of Pep-GaMD simulations, we did not observe the enzyme activation at other cleavage sites except for ζ cleavage at the amide bond between Val46-Ile47 of Aβ49 peptide. This can be observed from the time course plots of the distance between the protonated Asp257 and the carbonyl oxygen atoms of residues Ile47 (for cleavage at the second position) and Ile45 (for cleavage at the fourth position) (**Figure S21**). Moreover, the pathway of tripeptide trimming for ζ activation is energetically more favorable compared to that of the second or fourth amino acid residue cleavage. In this context, even though Pep-GaMD was able to capture the slow dynamic transitions of the enzyme activation for ζ cleavage during 600 ns simulation time, the simulations appeared to still suffer from insufficient sampling of the entire system conformational space and the calculated free energy profiles remained un-converged. Hence, the free energy profiles reflect semi-quantitative picture of the tripeptide trimming process rather than the exact correctness of the free energy values.

Here, we have investigated both the wildtype and 5 FAD mutants (including I45F, A42T, V46F, I45T and T48P) of the substrate. In a recent report[31], we determined the Aβ42/40 ratios for these and other FAD mutations in APP substrate and found the relative effects of these mutations on this ratio compared to that seen with WT enzyme to be generally consistent with those reported from other groups[36-38, 45]. To the best of our knowledge, there are no other studies comprehensively exploring APP FAD mutations and how they are processed by γ-secretase beyond our own[31]. Even with respect to Aβ42/40 ratios, a standard measure in the field, the only other comprehensive study of the 14 APP TMD FAD mutations was by our group[10], which gave closely similar relative changes in Aβ42/40 ratios with all these mutations, even though the systems were different (cellular transfection of APP[10] vs. C100Flag and purified proteins[31]).

Other reports on effects of APP mutations on Aβ42/40 have studied only very selected mutations. Among the 5 mutations studied in the current work: (1) Aβ42 levels cannot be determined by ELISA for A42T, as this changes the ELISA epitope; (2) No reported data can be found for T48P; Similar Aβ42/40 changes are seen with I45F and I45T[36-38]; The only discrepancy is with V46F: Devkota et al.[31] showed no change vs. WT, while Bolduc et. al.[10], Lichtenthaler et. al.[37], and Tamaoka et. al.[45] report ~4-fold increases in Aβ42/40. The reason for this discrepancy is unclear, however, only Devkota et. al. [31] used purified proteins, while the other reports measured secreted peptides in transfected cells.

In summary, we have presented here the first dynamic model of tripeptide trimming—of Aβ49 to Aβ46—by γ-secretase, which was highly consistent with mass spectrometry (MS) and western blotting biochemical experiments. Specifically, MS and western blotting were used to quantify the efficiency of tripeptide trimming of WT and FAD mutant Aβ49. In comparison to WT Aβ49, the efficiency of tripeptide trimming was similar for the I45F, A42T and V46F Aβ49 FAD

mutants, but substantially diminished for the I45T and T48P mutants. All-atom simulations performed in parallel with the biochemical experiments captured remarkable structural rearrangements of both the enzyme and substrate, in which hydrogen-bonded catalytic aspartates and water became poised for tripeptide trimming of Aβ49 to Aβ46. Our complementary biochemical experiments and all-atom simulations have enabled elucidation of the mechanism of tripeptide trimming of γ-secretase. It will guide our future studies on subsequent cleavage steps of the APP substrate and processive cleavage of the other substrates of γ-secretase. Detailed mechanistic understanding of these processes is expected to greatly facilitate rational drug design of this critical enzyme.

Associated Content

Supporting Information

Supplementary file containing **Materials and Methods, Supporting Figures S1 - S20**, **Supporting Table S1 – S2** and **Supporting Movies Captions**. The Supporting Information is available free of charge on the ACS Publications website.

Acknowledgements

This work used supercomputing resources with allocation award TG-MCB180049 through the Extreme Science and Engineering Discovery Environment (XSEDE), which is supported by National Science Foundation grant number ACI-1548562, and project M2874 through the National Energy Research Scientific Computing Center (NERSC), which is a U.S. Department of Energy Office of Science User Facility operated under Contract No. DE-AC02-05CH11231, and the

Research Computing Cluster at the University of Kansas. This work was supported in part by the startup funding in the College of Liberal Arts and Sciences at the University of Kansas (Y.M.) and GM122894 from the National Institutes of Health (M.S.W.).

Competing Interests Statement

There are no competing interests.

References

1. Weller, J.; Budson, A., Current understanding of Alzheimer's disease diagnosis and treatment. *F1000Research* **2018,** *7*, F1000 Faculty Rev-1161.
2. Funamoto, S.; Tagami, S.; Okochi, M.; Morishima-Kawashima, M. In *Successive cleavage of β-amyloid precursor protein by γ-secretase*, Seminars in cell & developmental biology, Elsevier: 2020; pp 64-74.
3. Hemming, M. L.; Elias, J. E.; Gygi, S. P.; Selkoe, D. J., Proteomic Profiling of gamma-Secretase Substrates and Mapping of Substrate Requirements. *Plos Biol* **2008,** *6* (10), 2314-2328.
4. Guner, G.; Lichtenthaler, S. F., The substrate repertoire of gamma-secretase/presenilin. *Semin Cell Dev Biol* **2020,** *105*, 27-42.
5. Gu, Y.; Misonou, H.; Sato, T.; Dohmae, N.; Takio, K.; Ihara, Y., Distinct intramembrane cleavage of the β-amyloid precursor protein family resembling γ-secretase-like cleavage of Notch. *Journal of Biological Chemistry* **2001,** *276* (38), 35235-35238.
6. Qi-Takahara, Y.; Morishima-Kawashima, M.; Tanimura, Y.; Dolios, G.; Hirotani, N.; Horikoshi, Y.; Kametani, F.; Maeda, M.; Saido, T. C.; Wang, R.; Ihara, Y., Longer forms of amyloid beta protein: implications for the mechanism of intramembrane cleavage by gamma-secretase. *J Neurosci* **2005,** *25* (2), 436-45.
7. Takami, M.; Nagashima, Y.; Sano, Y.; Ishihara, S.; Morishima-Kawashima, M.; Funamoto, S.; Ihara, Y., gamma-Secretase: successive tripeptide and tetrapeptide release from the transmembrane domain of beta-carboxyl terminal fragment. *J Neurosci* **2009,** *29* (41), 13042-52.
8. Selkoe, D. J.; Hardy, J., The amyloid hypothesis of Alzheimer's disease at 25 years. *EMBO molecular medicine* **2016,** *8* (6), 595-608.
9. Tanzi, R. E., The genetics of Alzheimer disease. *Cold Spring Harbor perspectives in medicine* **2012,** *2* (10), a006296.
10. Bolduc, D. M.; Montagna, D. R.; Seghers, M. C.; Wolfe, M. S.; Selkoe, D. J., The amyloid-beta forming tripeptide cleavage mechanism of γ-secretase. *Elife* **2016,** *5*, e17578.
11. Yang, G.; Zhou, R.; Zhou, Q.; Guo, X.; Yan, C.; Ke, M.; Lei, J.; Shi, Y., Structural basis of Notch recognition by human γ-secretase. *Nature* **2019,** *565* (7738), 192-197.
12. Zhou, R.; Yang, G.; Guo, X.; Zhou, Q.; Lei, J.; Shi, Y., Recognition of the amyloid precursor protein by human γ-secretase. *Science* **2019,** *363* (6428), eaaw0930.
13. Hitzenberger, M.; Zacharias, M., Structural Modeling of gamma-Secretase A beta(n) Complex Formation and Substrate Processing. *Acs Chem Neurosci* **2019,** *10* (3), 1826-1840.
14. Götz, A.; Mylonas, N.; Högel, P.; Silber, M.; Heinel, H.; Menig, S.; Vogel, A.; Feyrer, H.; Huster, D.; Luy, B., Modulating hinge flexibility in the APP transmembrane domain alters γ-secretase cleavage. *Biophysical journal* **2019,** *116* (11), 2103-2120.
15. Dehury, B.; Tang, N.; Kepp, K. P., Molecular dynamics of C99-bound γ-secretase reveal two binding modes with distinct compactness, stability, and active-site retention: implications for Aβ production. *Biochemical Journal* **2019,** *476* (7), 1173-1189.
16. Somavarapu, A. K.; Kepp, K. P., Membrane dynamics of γ-secretase provides a molecular basis for β-amyloid binding and processing. *Acs Chem Neurosci* **2017,** *8* (11), 2424-2436.
17. Götz, A.; Högel, P.; Silber, M.; Chaitoglou, I.; Luy, B.; Muhle-Goll, C.; Scharnagl, C.; Langosch, D., Increased H-Bond Stability Relates to Altered ε-Cleavage Efficiency and Aβ Levels in the I45T Familial Alzheimer's Disease Mutant of APP. *Scientific reports* **2019,** *9* (1), 1-12.
18. Hitzenberger, M.; Zacharias, M., gamma-Secretase Studied by Atomistic Molecular Dynamics Simulations: Global Dynamics, Enzyme Activation, Water Distribution and Lipid Binding. *Front Chem* **2019,** *6*, 640.

19. Aguayo-Ortiz, R.; Chavez-Garcia, C.; Straub, J. E.; Dominguez, L., Characterizing the structural ensemble of gamma-secretase using a multiscale molecular dynamics approach. *Chem Sci* **2017,** *8* (8), 5576-5584.
20. Lee, J. Y.; Feng, Z.; Xie, X. Q.; Bahar, I., Allosteric Modulation of Intact gamma-Secretase Structural Dynamics. *Biophys J* **2017,** *113* (12), 2634-2649.
21. Gertsik, N.; Ende, C. W. A.; Geoghegan, K. F.; Nguyen, C.; Mukherjee, P.; Mente, S.; Seneviratne, U.; Johnson, D. S.; Li, Y. M., Mapping the Binding Site of BMS-708163 on gamma-Secretase with Cleavable Photoprobes. *Cell Chem Biol* **2017,** *24* (1), 3-8.
22. Petit, D.; Hitzenberger, M.; Lismont, S.; Zoltowska, K. M.; Ryan, N. S.; Mercken, M.; Bischoff, F.; Zacharias, M.; Chávez-Gutiérrez, L., Extracellular interface between APP and Nicastrin regulates Aβ length and response to γ-secretase modulators. *The EMBO journal* **2019,** *38* (12), e101494.
23. Hitzenberger, M.; Zacharias, M., Uncovering the Binding Mode of γ-Secretase Inhibitors. *Acs Chem Neurosci* **2019,** *10* (8), 3398-3403.
24. Dehury, B.; Somavarapu, A. K.; Kepp, K. P., A computer-simulated mechanism of familial Alzheimer's disease: Mutations enhance thermal dynamics and favor looser substrate-binding to γ-secretase. *Journal of Structural Biology* **2020,** *212* (3), 107648.
25. Dehury, B.; Tang, N.; Mehra, R.; Blundell, T. L.; Kepp, K. P., Side-by-side comparison of Notch-and C83 binding to γ-secretase in a complete membrane model at physiological temperature. *RSC Advances* **2020,** *10* (52), 31215-31232.
26. Chen, S.-Y.; Zacharias, M., How mutations perturb γ-secretase active site studied by free energy simulations. *Acs Chem Neurosci* **2020,** *11* (20), 3321-3332.
27. Soto-Ospina, A.; Araque Marín, P.; Bedoya, G.; Sepulveda-Falla, D.; Villegas Lanau, A., Protein Predictive Modeling and Simulation of Mutations of Presenilin-1 Familial Alzheimer's Disease on the Orthosteric Site. *Frontiers in molecular biosciences* **2021,** *8*, 387.
28. Orzeł, U.; Jakowiecki, J.; Młynarczyk, K.; Filipek, S., The Role of Cholesterol in Amyloidogenic Substrate Binding to the γ-Secretase Complex. *Biomolecules* **2021,** *11* (7), 935.
29. Bhattarai, A.; Devkota, S.; Bhattarai, S.; Wolfe, M. S.; Miao, Y., Mechanisms of gamma-Secretase Activation and Substrate Processing. *ACS Cent Sci* **2020,** *6* (6), 969-983.
30. Miao, Y.; Feher, V. A.; McCammon, J. A., Gaussian Accelerated Molecular Dynamics: Unconstrained Enhanced Sampling and Free Energy Calculation. *Journal of Chemical Theory and Computation* **2015,** *11* (8), 3584-3595.
31. Devkota, S.; Williams, T. D.; Wolfe, M. S., Familial Alzheimer's disease mutations in amyloid protein precursor alter proteolysis by γ-secretase to increase amyloid β-peptides of≥ 45 residues. *Journal of Biological Chemistry* **2021,** *296*, 100281.
32. Kamp, F.; Winkler, E.; Trambauer, J.; Ebke, A.; Fluhrer, R.; Steiner, H., Intramembrane proteolysis of β-amyloid precursor protein by γ-secretase is an unusually slow process. *Biophysical journal* **2015,** *108* (5), 1229-1237.
33. Wang, J.; Miao, Y., Peptide Gaussian accelerated molecular dynamics (Pep-GaMD): Enhanced sampling and free energy and kinetics calculations of peptide binding. *The Journal of Chemical Physics* **2020,** *153* (15), 154109.
34. Xue, Y.; Yuwen, T.; Zhu, F.; Skrynnikov, N. R., Role of electrostatic interactions in binding of peptides and intrinsically disordered proteins to their folded targets. 1. NMR and MD characterization of the complex between the c-Crk N-SH3 domain and the peptide Sos. *Biochemistry* **2014,** *53* (41), 6473-6495.
35. Li, Y.-M.; Lai, M.-T.; Xu, M.; Huang, Q.; DiMuzio-Mower, J.; Sardana, M. K.; Shi, X.-P.; Yin, K.-C.; Shafer, J. A.; Gardell, S. J., Presenilin 1 is linked with γ-secretase activity in the detergent solubilized state. *Proceedings of the National Academy of Sciences* **2000,** *97* (11), 6138-6143.

36. Herl, L.; Thomas, A. V.; Lill, C. M.; Banks, M.; Deng, A.; Jones, P. B.; Spoelgen, R.; Hyman, B. T.; Berezovska, O., Mutations in amyloid precursor protein affect its interactions with presenilin/γ-secretase. *Molecular and Cellular Neuroscience* **2009,** *41* (2), 166-174.
37. Lichtenthaler, S. F.; Wang, R.; Grimm, H.; Uljon, S. N.; Masters, C. L.; Beyreuther, K., Mechanism of the cleavage specificity of Alzheimer's disease γ-secretase identified by phenylalanine-scanning mutagenesis of the transmembrane domain of the amyloid precursor protein. *Proceedings of the National Academy of Sciences* **1999,** *96* (6), 3053-3058.
38. Suárez-Calvet, M.; Belbin, O.; Pera, M.; Badiola, N.; Magrané, J.; Guardia-Laguarta, C.; Muñoz, L.; Colom-Cadena, M.; Clarimón, J.; Lleó, A., Autosomal-dominant Alzheimer's disease mutations at the same codon of amyloid precursor protein differentially alter Aβ production. *Journal of neurochemistry* **2014,** *128* (2), 330-339.
39. Roe, D. R.; Cheatham, T. E., PTRAJ and CPPTRAJ: Software for Processing and Analysis of Molecular Dynamics Trajectory Data. *Journal of Chemical Theory and Computation* **2013,** *9* (7), 3084-3095.
40. Dubois, B.; Feldman, H. H.; Jacova, C.; Hampel, H.; Molinuevo, J. L.; Blennow, K.; DeKosky, S. T.; Gauthier, S.; Selkoe, D.; Bateman, R., Advancing research diagnostic criteria for Alzheimer's disease: the IWG-2 criteria. *The Lancet Neurology* **2014,** *13* (6), 614-629.
41. Quintero-Monzon, O.; Martin, M. M.; Fernandez, M. A.; Cappello, C. A.; Krzysiak, A. J.; Osenkowski, P.; Wolfe, M. S., Dissociation between the Processivity and Total Activity of gamma-Secretase: Implications for the Mechanism of Alzheimer's Disease-Causing Presenilin Mutations. *Biochemistry* **2011,** *50* (42), 9023-9035.
42. Fernandez, M. A.; Klutkowski, J. A.; Freret, T.; Wolfe, M. S., Alzheimer Presenilin-1 Mutations Dramatically Reduce Trimming of Long Amyloid beta-Peptides (A beta) by gamma-Secretase to Increase 42-to-40-Residue A beta. *Journal of Biological Chemistry* **2014,** *289* (45), 31043-31052.
43. Yang, G.; Zhou, R.; Guo, X.; Yan, C.; Lei, J.; Shi, Y., Structural basis of gamma-secretase inhibition and modulation by small molecule drugs. *Cell* **2021,** *184* (2), 521-533 e14.
44. Güner, G.; Lichtenthaler, S. F. In *The substrate repertoire of γ-secretase/presenilin*, Seminars in Cell & Developmental Biology, Elsevier: 2020.
45. Tamaoka, A.; Odaka, A.; Ishibashi, Y.; Usami, M.; Sahara, N.; Suzuki, N.; Nukina, N.; Mizusawa, H.; Shoji, S. i.; Kanazawa, I., APP717 missense mutation affects the ratio of amyloid beta protein species (A beta 1-42/43 and a beta 1-40) in familial Alzheimer's disease brain. *Journal of Biological Chemistry* **1994,** *269* (52), 32721-32724.

Table 1: Summary of Pep-GaMD simulations performed on different systems of γ-secretase bound by Aβ49 and AICD50-99 peptides. [a]N_{atoms} is the total number of atoms in the simulation systems. [b]ΔV_{avg} and [c]$\sigma_{\Delta V}$ are the average and standard deviation of the Pep-GaMD boost potential, respectively.

System	[a]N_{atoms}	Dimension (Å^3)	Simulation (ns)	[b]ΔV_{avg} (kcal/mol)	[c]$s_{\Delta v}$ (kcal/mol)
WT Aβ49	254,233	152 x 123 x 146	600 x 3	106.9	14.0
WT neutral Aβ49 - neutral AICD	254,337	152 x 123 x 146	600 x 3	155.9	11.8
WT neutral Aβ49 - charged AICD	254,340	152 x 123 x 146	600 x 3	134.2	11.3
WT charged Aβ49 - neutral AICD	254,334	152 x 123 x 146	600 x 3	133.9	11.1
WT charged Aβ49 - charged AICD	254,377	152 x 123 x 146	600 x 3	134.0	10.9
I45F charged Aβ49 - charged AICD	254,335	152 x 123 x 146	600 x 3	137.5	12.1
A42T charged Aβ49 - charged AICD	254,341	152 x 123 x 146	600 x 3	148.9	11.4
V46F charged Aβ49 - charged AICD	254,329	152 x 123 x 146	600 x 3	177.9	11.9
I45T charged Aβ49 - charged AICD	254,323	152 x 123 x 146	600 x 3	149.2	11.4
T48P charged Aβ49 - charged AICD	254,328	152 x 123 x 146	600 x 3	137.9	11.2

Figure Captions

Figure 1: Tripeptide trimming of the wildtype (WT) and FAD mutants of Aβ49 γ-secretase characterized by MS, western blotting and Pep-GaMD simulations. (A) MALDI-TOF MS detection of AICD 50-99 and AICD 49-99 products, (B) Anti-FLAG immunoblot of total AICD-FLAG levels. Purified C100-FLAG at a range of known concentrations was used to generate a standard curve, (C) Quantification of total AICD-FLAG levels from immunoblot by densitometry, (D) Quantification of AICD 50-99 using total AICD levels determined from immunoblot and intensity ratios determined from MALDI-TOF MS, (E) Quantification of ITL tripeptides generated from trimming of WT and FAD mutants of Aβ49, (F) Cleavage efficiency of the first trimming (ζ) step. Grey dotted line denotes cleavage efficiency from WT APP substrate. (G-L) 2D free energy profiles calculated from the Pep-GaMD simulations of (G) WT, (H) I45F, (I) A42T, (J) V46F, (K) I45T and (L) T48P Aβ49 bound to γ-secretase. The distances between the Cγ atoms of Asp257 and Asp385 in PS1 and between the hydroxyl oxygen of PS1 Asp257 and the carbonyl oxygen of Aβ49 Leu49 were selected as the reaction coordinates.

Figure 2: Conformational changes of the PS1 catalytic subunit and substrate during activation of γ-secretase for tripeptide trimming of Aβ49 in Pep-GaMD simulations. (A) Comparison of the Initial (active for ε cleavage, blue) and Final (active for ζ cleavage, red) conformations of the Aβ49-bound PS1. The enzyme activation for the tripeptide trimming was characterized by coordinated hydrogen bonding between the enzyme Asp257, carbonyl oxygen of Aβ49 Val46 and a water molecule accommodated between the two aspartates poised for cleavage of the amide bond between Val46 and Ile47 residues. (B-F) Conformational changes of (B) Aβ49 substrate, (C) catalytic aspartates, (D) TM3, (E) TM6 and TM6a, and (F) β2 strand from the Initial to the Final conformational state. The helical domain of Aβ49 tilted by ~50º and residue Leu49 at

the C-terminus of Aβ49 moved downwards by ~5 Å. Protonated catalytic Asp257 moved ~3 Å towards the Aβ49 substrate. The enzyme TM3 moved outwards by ~2 Å and TM6a moved downwards by ~2 Å. The enzyme β2 strand (N-terminus of TM7) moved away from APP and closer towards the β1 strand (C-terminus of TM6a) by ~5 Å.

Figure 3: Time-dependent secondary structures of Aβ49 bound to γ-secretase calculated from the Pep-GaMD simulations. (A) WT, (B) I45F, (C) A42T and (D) V46F systems of Aβ49. Results from other simulations are plotted in **Figs. S12 and S15**.

Figure 4: Active-site conformations of γ-secretase for tripeptide trimming of Aβ49 observed in the Pep-GaMD simulations. (A-D) Conformations of the substrate P1', P2' and P3' residues in the Final active conformations of the (A) WT (red), (B) I45F (pink), (C) A42T (green) and (D) V46F (cyan) Aβ49 systems. (E) Comparison of the PS1 active-site S1', S2' and S3' pockets that accommodate the WT and mutants of Aβ49.

Figure 5: Dynamic model of tripeptide trimming of Aβ49 by γ-secretase. (A) The "Initial" conformational state of Aβ49 bound γ-secretase. (B) The WT Aβ49 and its I45F, A42T and V46F mutants were able to transition to the "Final" state with ~50° tilting of the helical domain and unwinding of the helix C-terminus (residues V44-I45) and became poised for ζ cleavage of the V46-I47 amide bond by γ-secretase. (C) In contrast, the I45T and T48P mutant Aβ49-bound γ-secretase were trapped in the "Intermediate" or "Inhibited-1" state, being inactive for ζ cleavage of the substrate.

Figure 1

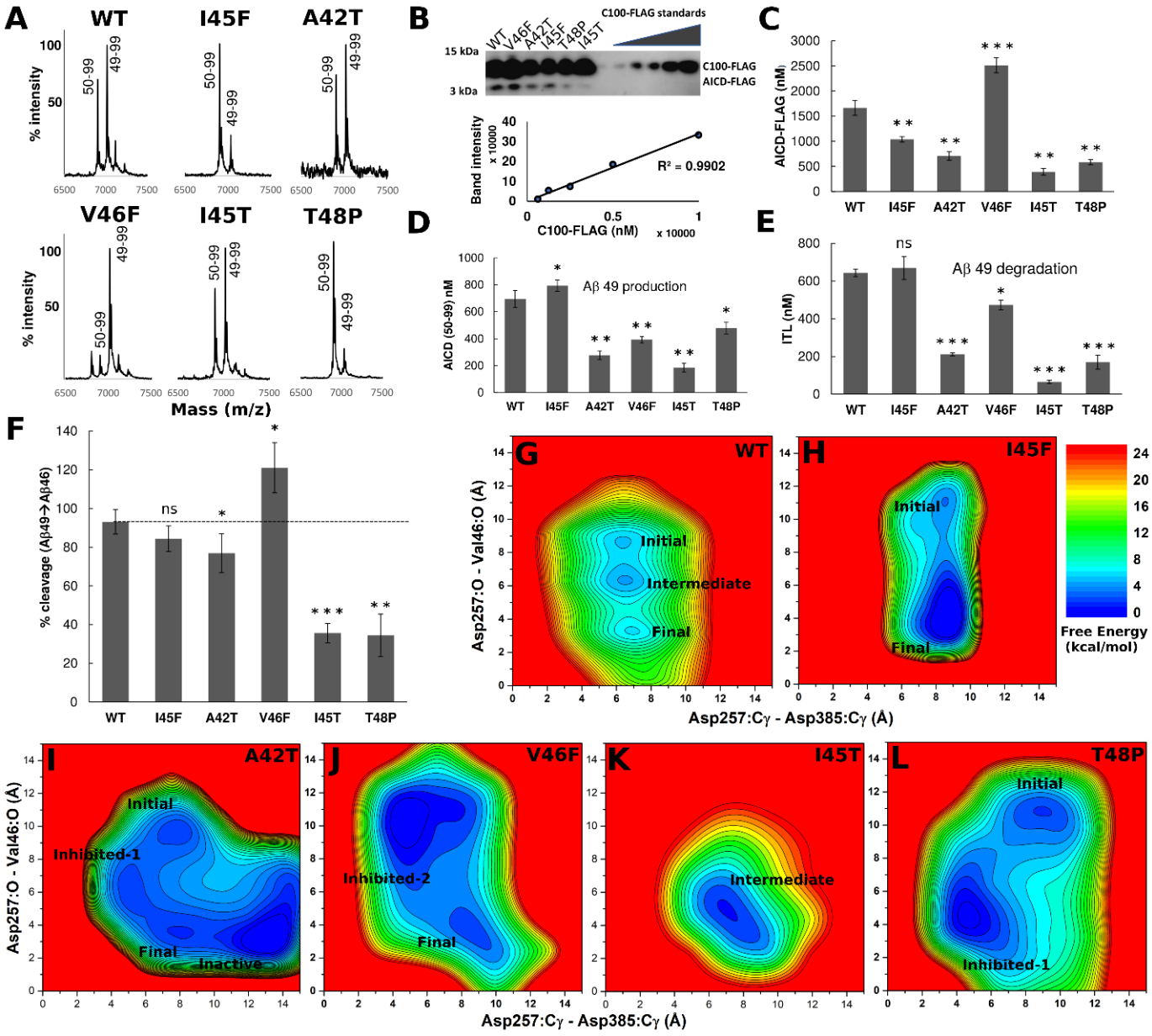
A
WT
I45F
A42T
V46F
I45T
T48P
% intensity
50-99
49-99
Mass (m/z)
B
C100-FLAG standards
15 kDa
3 kDa
C100-FLAG
AICD-FLAG
Band intensity x 10000
R² = 0.9902
C100-FLAG (nM) x 10000
C
AICD-FLAG (nM)
D
Aβ 49 production
AICD (50-99) nM
E
Aβ 49 degradation
ns
ITL (nM)
F
% cleavage (Aβ49→Aβ46)
G
WT
H
I45F
Initial
Intermediate
Final
Asp257:O - Val46:O (Å)
Asp257:Cγ - Asp385:Cγ (Å)
Free Energy (kcal/mol)
I
A42T
Inhibited-1
Inactive
J
V46F
Inhibited-2
K
I45T
L
T48P

Figure 2

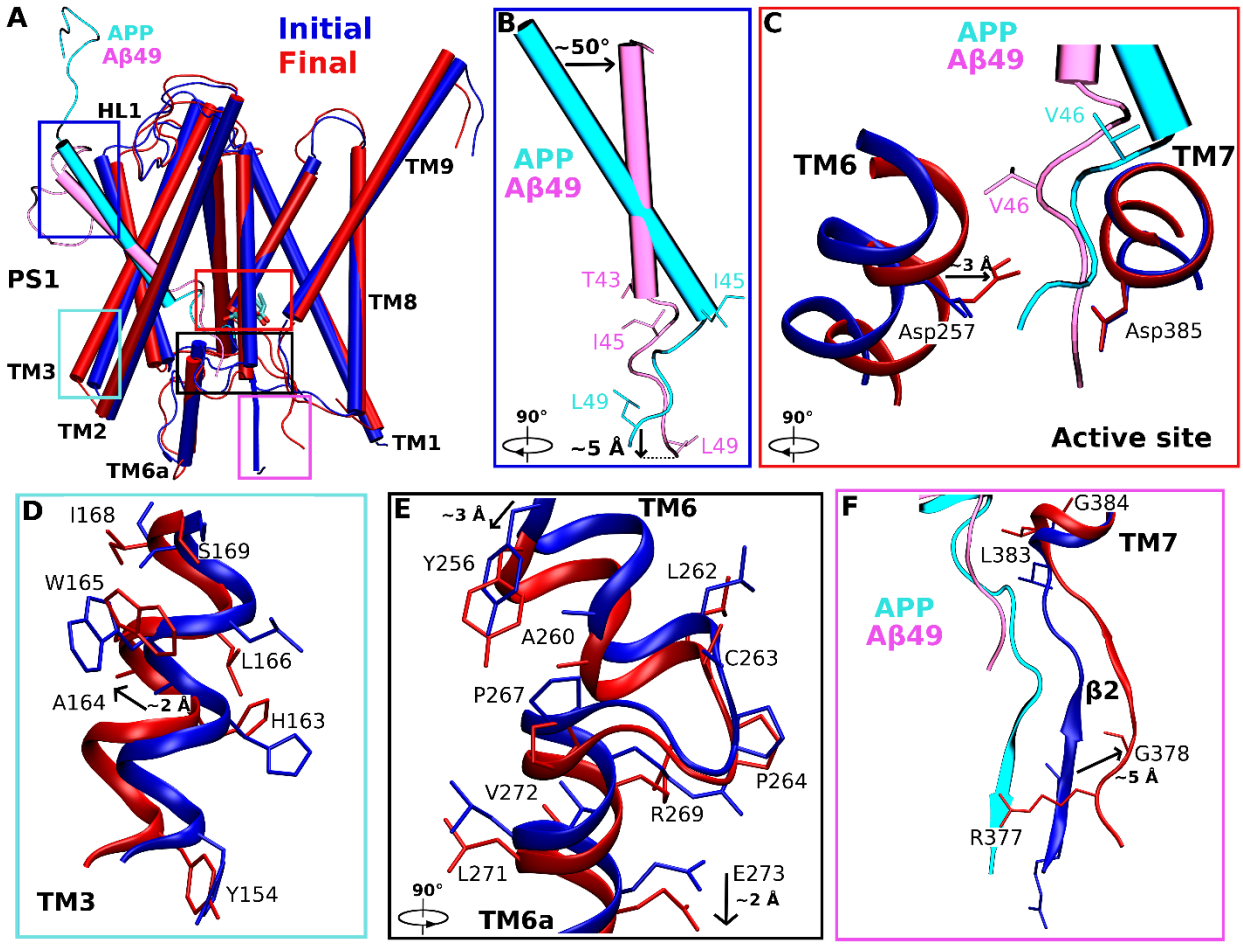
A
APP
Aβ49
Initial
Final
HL1
TM9
PS1
TM8
TM3
TM2
TM6a
TM1
B
~50°
APP
Aβ49
T43
I45
I45
L49
90°
~5 Å
L49
C
APP
Aβ49
V46
TM6
TM7
V46
~3 Å
Asp257
Asp385
90°
Active site
D
I168
S169
W165
L166
A164
~2 Å
H163
TM3
Y154
E
~3 Å
TM6
Y256
L262
A260
C263
P267
P264
V272
R269
L271
E273
~2 Å
90°
TM6a
F
G384
TM7
L383
APP
Aβ49
β2
G378
~5 Å
R377

Figure 3

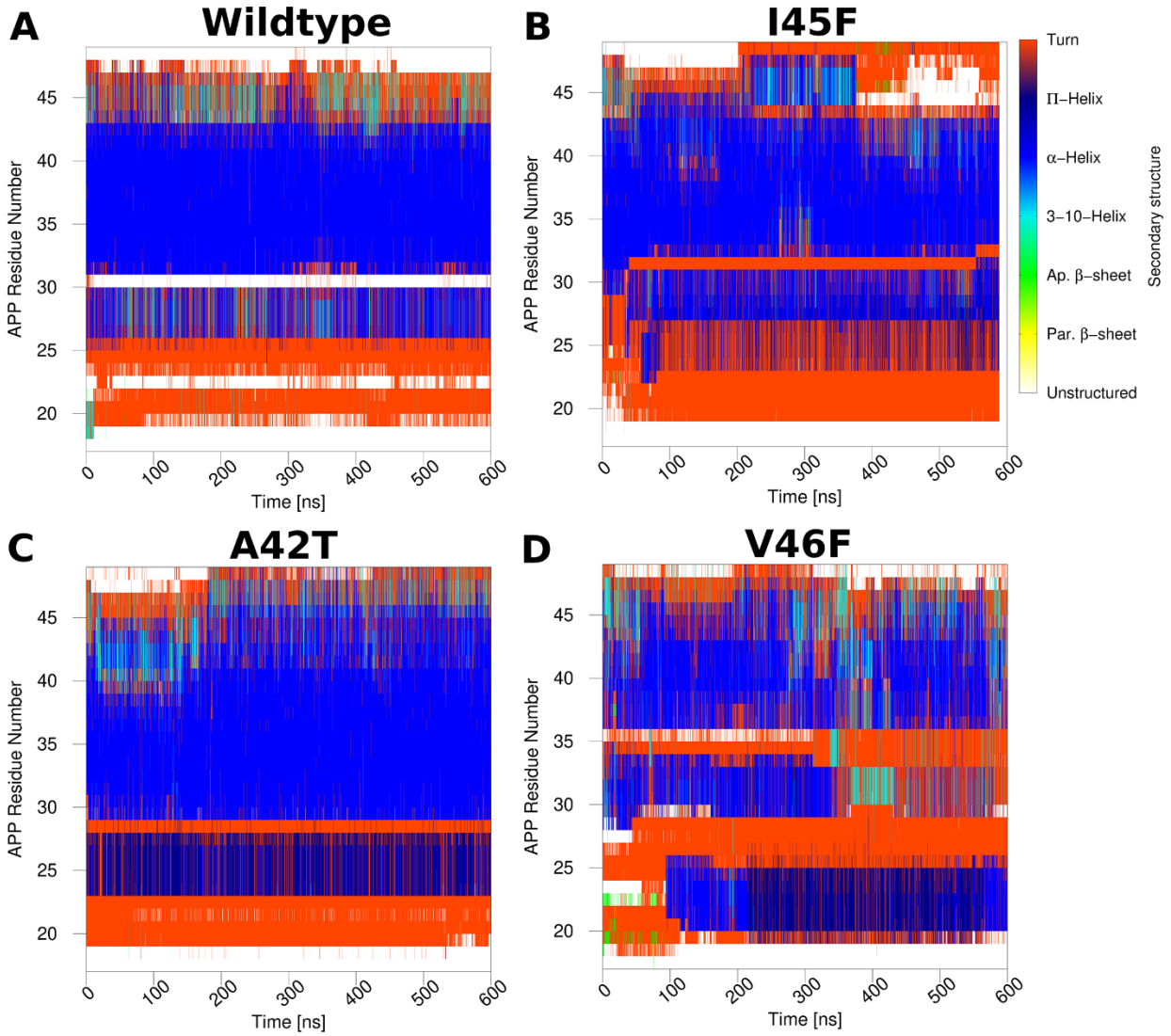
A
Wildtype
B
I45F
C
A42T
D
V46F
APP Residue Number
Time [ns]
Turn
Π–Helix
α–Helix
3–10–Helix
Ap. β–sheet
Par. β–sheet
Unstructured
Secondary structure

Figure 4

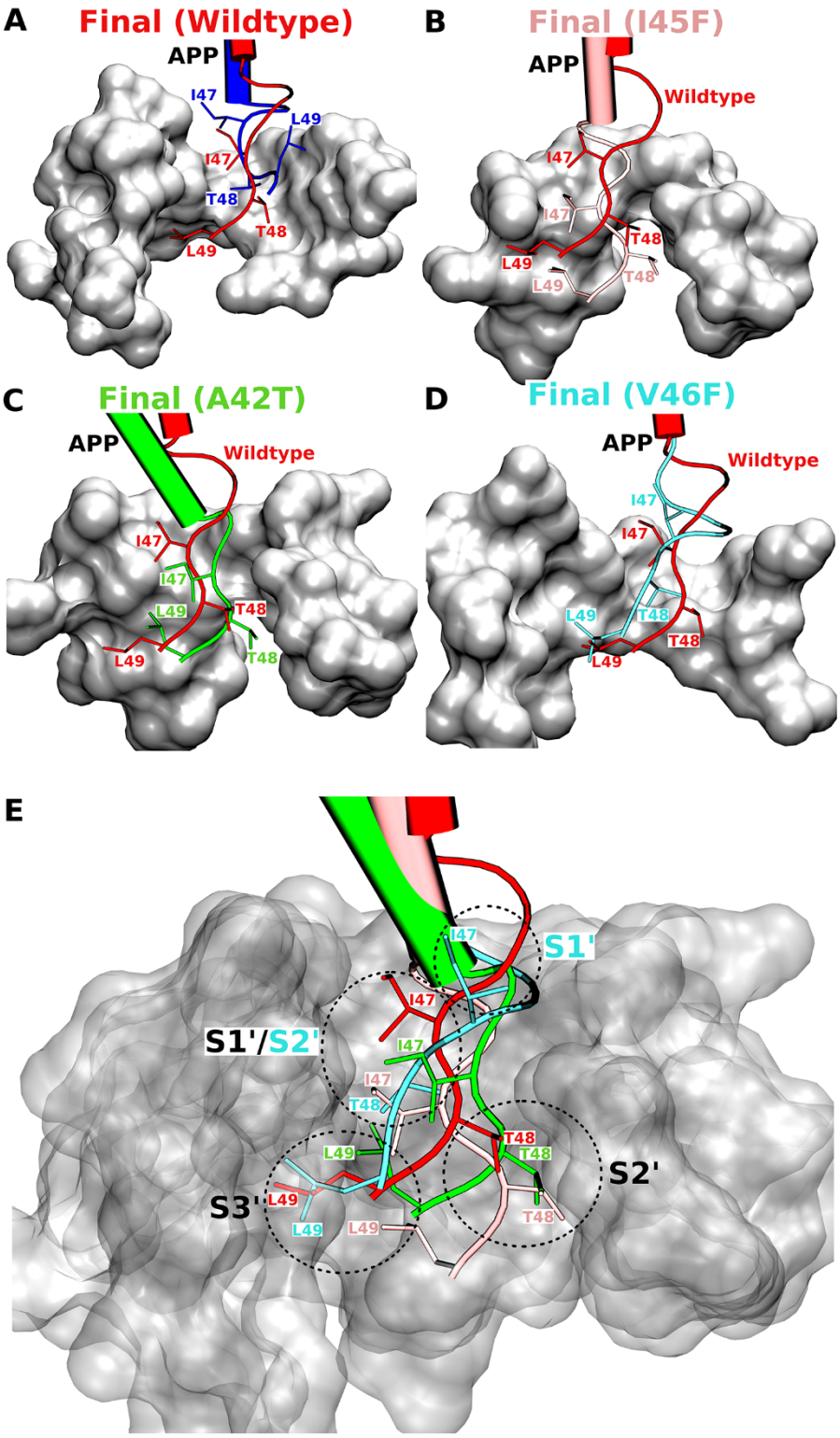
A
Final (Wildtype)
APP
I47
L49
I47
T48
T48
L49
B
Final (I45F)
APP
Wildtype
I47
I47
T48
L49
L49
T48
C
Final (A42T)
APP
Wildtype
I47
I47
L49
T48
L49
T48
D
Final (V46F)
APP
Wildtype
I47
I47
L49
T48
T48
L49
E
I47
S1'
I47
S1'/S2'
I47
I47
T48
T48
T48
L49
S2'
S3'
L49
L49
L49
T48

Figure 5

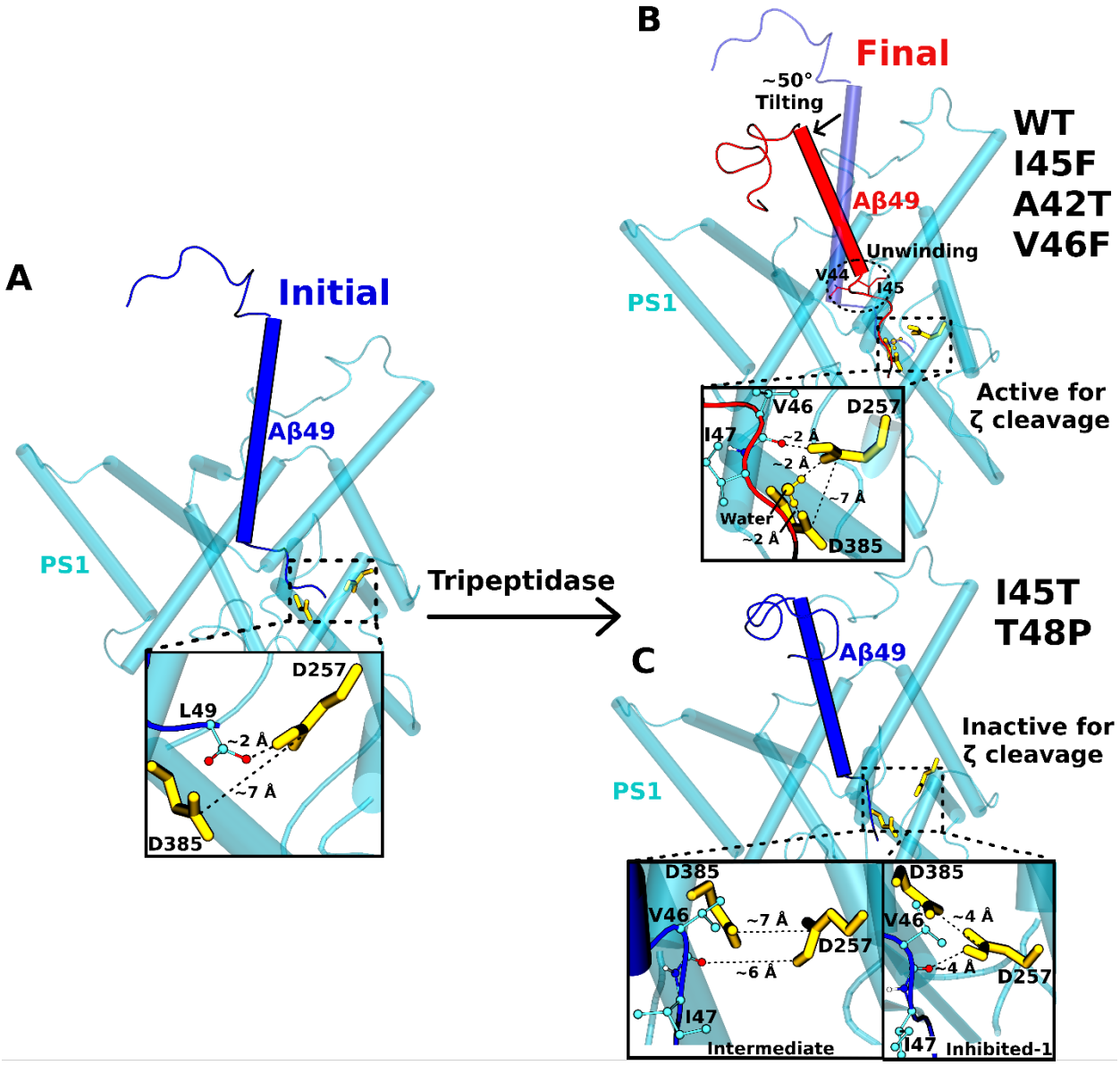
A
Initial
Aβ49
PS1
D257
L49
~2 Å
~7 Å
D385
Tripeptidase
B
Final
~50°
Tilting
Aβ49
Unwinding
V44
I45
PS1
WT
I45F
A42T
V46F
Active for
ζ cleavage
V46
D257
I47
~2 Å
~2 Å
~7 Å
Water
~2 Å
D385
C
I45T
T48P
Aβ49
Inactive for
ζ cleavage
PS1
D385
V46
~7 Å
D257
~6 Å
I47
Intermediate
D385
V46
~4 Å
~4 Å
D257
I47
Inhibited-1

Table of Contents/Abstract Graphics

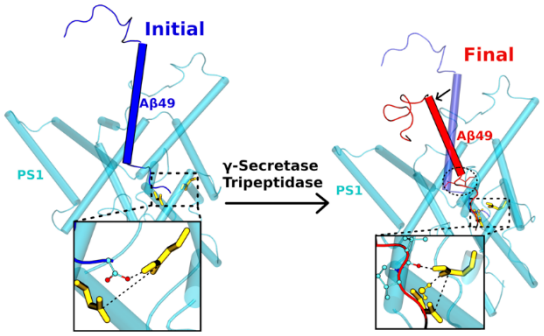

Complimentary accelerated molecular simulations, mass spectrometry and western blotting experiments have revealed the dynamic mechanism of tripeptide trimming of wildtype and familial Alzheimer's disease (FAD) Aβ49 mutants by γ-secretase. In comparison to wildtype Aβ49, the efficiency of tripeptide trimming was similar for the I45F, A42T and V46F Aβ49, but substantially diminished for the I45T and T48P mutants.

Supporting Information

Mechanism of Tripeptide Trimming of Amyloid β-Peptide 49 by γ-Secretase

Apurba Bhattarai[1], Sujan Devkota[2], Hung Nguyen Do[1], Jinan Wang[1], Sanjay Bhattarai[2], Michael S. Wolfe[2]* and Yinglong Miao[1]*

[1]Center for Computational Biology and Department of Molecular Biosciences,

[2]Department of Medicinal Chemistry, School of Pharmacy, University of Kansas, Lawrence, KS 66047, USA

* Corresponding emails: mswolfe@ku.edu, miao@ku.edu

Table of Contents:

Materials and Method

C100-FLAG substrates expression and purification

C100-FLAG constructs [1] were transformed into *E. coli* BL21 cells. *E. coli* BL21 cells were grown in LB media at 37^0C in the incubator shaker until OD_{600} reached 0.6. Cells were induced with 0.5 mM IPTG and grown for 4 hours shaking at 37 ºC. The cells were then pelleted and resuspended in lysis buffer composed of 50 mM HEPES pH 8 with 1% Triton X-100. The cells were lysed by French press three times and lysate was centrifuged to remove cell debris. The clear lysate was mixed with anti-FLAG M2-agarose beads (Sigma-Aldrich) for 16 h at 4 ºC. Substrates were eluted from the beads with 100 mM glycine pH 2.5 with 0.25% NP-40, following by washing of the beads 3 times with lysis buffer. The elute was neutralized with Tris HCl and stored at -80^0C.

γ-Secretase assays

γ-Secretase purification and assays were carried out as described previously [2]. Briefly, 30 nM γ-secretase was incubated for 30 min at 37 °C in assay buffer composed of 50 mM Hepes pH 7.0, 150 mM NaCl, and 0.25% 3-[(3-cholamidopropyl)dimethylammonio]-2-hydroxy-1-propanesulfonate (CHAPSO) detergent supplemented with 0.1% phosphatidylcholine (DOPC) and 0.025% phosphatidylethanolamine (DOPE). Reactions were initiated by addition purified C100-FLAG substrate to a final concentration of 5 μM and performed by incubating at 37 °C for 16 h.

The enzymes used for all reactions were purified wild-type γ-secretase from the same enzyme preparation. Essentially, all of the purified enzymes were active, as determined using a

stoichiometric γ-secretase inhibitor. There was no loss of specific activity, and any reduction in endoproteolytic cleavage of APP substrate or subsequent tripeptide trimming was due to the mutation in the substrate. Each substrate was purified to homogeneity and analyzed for its integrity and identity as we have recently reported[3]. Moreover, all enzyme reactions were conducted under substrate saturation and at a time point within the linear range of product formation (i.e., product levels are proportional to reaction rates).

Detection of AICD species

After 16 h, AICD-FLAG produced from the enzymatic assay was isolated by immunoprecipitation. The assay mixture was incubated with anti-FLAG M2 beads (SIGMA) in 10 mM MES pH 6.5, 10 mM NaCl, 0.05% DDM detergent for 16 h at 4 ^{o}C. AICD products were eluted from the anti-FLAG beads with acetonitrile:water (1:1) with 0.1% trifluoroacetic acid. The elutes were run on a Bruker autoflex MALDI-TOF mass spectrometer in linear mode.

Western blotting

Samples from γ-secretase assays and C100-FLAG standards were run on 4-12% Bis-Tris gel and transferred to PVDF membrane. The membrane was treated with 5% dry milk in PBS Tween-20 for 1 h at ambient temperature. The membrane was then incubated with anti-FLAG M2 antibodies at 4 ^{o}C overnight. The membrane was washed 3 times with PBS Tween-20 and incubated with anti-mouse secondary antibodies for 1 h. The membrane was washed and imaged for chemiluminescence and band signal intensity was measured by densitometry.

LC-MS/MS tandem mass spectrometry

Small peptides were analyzed using an ESI Quadrupole Time-of-Flight (Q-TOF) mass spectrometer (Q-TOF Premier, Waters) by LC-MS/MS experiment, as previously described [3]. Briefly, assay samples and standard peptides were loaded onto a C18 column and eluted with a step gradient of 0.08% aqueous formic acid (A), acetonitrile (B), isopropanol (C), and a 1:1 acetone/dioxane mixture (D). The gradient well separated the lipids and detergent present in the buffer from the small peptides. The three most abundant collision-induced dissociation (CID) fragments were identified from the MS/MS for each small peptide. The peptide chromatographic area was obtained from the summed signals from three most abundant ions.

Simulation system setup

All-atom simulations using the Pep-GaMD method[4] were performed on the γ-secretase activation for ζ cleavage of Aβ49. Active APP-bound γ-secretase was taken from the previous study[2] and the amide bond between Aβ49 and AICD50-99 was cleaved as the starting structure. The enzyme was based on previously published cryo-EM structure[5] **(Fig. S1)** with Asp385 computationally restored, artificial enzyme-substrate disulfide bond removed and missing residues on APP N-terminus added. The Ala385 residue in the cryo-EM structure was computationally mutated back to Asp385. Two artificial disulfide bonds between Cys112 of PS1-Q112C and Cys4 of PS1-V24C were removed as the wildtype residues were restored. SWISS-MODEL[6] homology modeling was used to restore 5 N-terminal APP residues that were missing in the cryo-EM structure. The simulation systems of γ-secretase bound by wildtype and mutant Aβ49 **(Figure S1)** were then

prepared similarly as in the previous study for APP-bound γ-secretase and summarized in **Table 1**. For APP-mutant simulations systems, isoleucine, alanine, valine, isoleucine and threonine residues were mutated to phenylalanine, threonine, phenylalanine, threonine and proline computationally at the 45^{th}, 42^{nd}, 46^{th}, 45^{th} and 48^{th} residue of APP substrate, respectively. These corresponded to I45F, A42T, V46F, I45T and T48P mutations as per the numbering based on C99, although the actual substrate in the model was based on C83.

In the Pep-GaMD simulations, boost potential was applied selectively to the essential potential energy of the peptide (Aβ49 and AICD50-99) to effectively model its high flexibility and accelerate its dynamic motions. In addition to the γ-secretase systems bound by charged C-terminal Aβ49 and charged N-terminal AICD50-99, and neutral C-terminal Aβ49 and charged N-terminal AICD50-99, we tested Pep-GaMD simulations on enzyme systems bound by Aβ49 in the absence and presence of charged C-terminal Aβ49 and neutral N-terminal AICD50-99, and neutral C-terminal Aβ49 and neutral N-terminal AICD50-99 **(Fig. S4)**. The neutral and charged N-terminus of the AICD50-99 was characterized by the presence of $-NH_2$ and NH_3^+ functional groups at the N-terminal end, respectively. Similarly, the neutral and charged C-terminus of Aβ49 was characterized by the presence of COOH and COO- functional groups at the C-terminal end, respectively. Unlike the charged N-terminal AICD50-99 systems, activation was not observed during the 600 ns of Pep-GaMD of either of the enzyme systems bound by Aβ49 in the absence and presence of neutral N-terminal AICD50-99 **(Figs. S6 and S8 and Table S2)**. Free energy profiles were plotted for the Pep-GaMD simulations of all these enzyme systems. Two low energy conformational states were identified in the system without the AICD bound including "Inhibited-2" and "Intermediate" **(Fig. S8A)**. Similarly, "Initial" and "Intermediate" low energy conformational states were identified in the free energy profile of the enzyme system bound to

charged C-terminal Aβ49 in the presence of neutral N-terminal AICD50-99 **(Fig. S8B)**. The free energy profile of γ-secretase system bound by neutral C-terminal Aβ49 in presence of neutral N-terminal AICD50-99 identified two low energy states including "Initial" and "Intermediate" **(Fig. S8C)**. "Final" and "Intermediate" low energy states were identified in the free energy profiles of the enzyme system bound by neutral C-terminal Aβ49 and charged N-terminal AICD50-99 **(Fig. S8D)**. The "Intermediate" and the "Inhibited-2" conformational states here were same as the one identified in the wildtype and the V46F mutant γ-secretase systems, respectively **(Fig. 2A and 2D)**. The "Initial" conformational state resembled the one identified in the wildtype, I45F and A42T mutant systems **(Fig. 2A-2C)**. In comparison, "Final" active conformational state was identified in the wildtype system bound to Aβ49 and charged N-terminal AICD50-99 **(Fig. 2A)**. Therefore, systems for γ-secretase bound by Aβ49 and charged N-terminal AICD50-99 were used for final Pep-GaMD simulations.

Simulation Protocol

The CHARMM36m[7] parameter set was used for the protein and POPC lipids. Initial energy minimization and thermalization of the γ-secretase complex followed the same protocol as used in the previous study[2]. Then dual-boost Pep-GaMD simulations were performed to investigate the γ-secretase enzyme activation for ζ cleavage (**Table 1**). The threshold energy E for adding boost potential was set to the upper bound, i.e., $E = V_{min} + (1/k)$[8-9]. The simulations included 50 ns equilibration after adding the boost potential and then multiple independent production runs lasting 600 ns with randomized initial atomic velocities. Pep-GaMD production simulation frames were saved every 0.2 ps for analysis.

Simulation analysis

VMD[10] and CPPTRAJ [11] were used to analyze the Pep-GaMD trajectories. The distance between the catalytic aspartates was calculated between the Cγ atoms. Hydrogen bond distance was calculated between the donor protonated oxygen atom of PS1 Asp257 and the acceptor carbonyl oxygen atom of APP substrate residue Val46. Root-mean-square fluctuations (RMSFs) were calculated for the protein residues, averaged over three independent Pep-GaMD simulations and color coded for schematic representation of each complex system. The CPPTRAJ was used to calculate the protein secondary structure plots. The *PyReweighting* toolkit[12] was applied to reweight Pep-GaMD simulations for free energy calculations by combining all simulation trajectories for each system. Bin size of 1-3 Å was used for the PMF calculation of distances. The cutoff was set to 500-1000 frames in each bin for calculating the 2D PMF profiles. Protein snapshots were taken every 1 ps for structural clustering. Clustering was performed on the Pep-GaMD simulations of wildtype, I45F, A42T and V46F mutant Aβ49 bound γ-secretase based on the RMSD of PS1 using hierarchical agglomerative algorithm in CPPTRAJ [11] generating ~10 representative structural clusters for each system. The top structural cluster was identified as the representative Final active conformational states for each γ-secretase system.

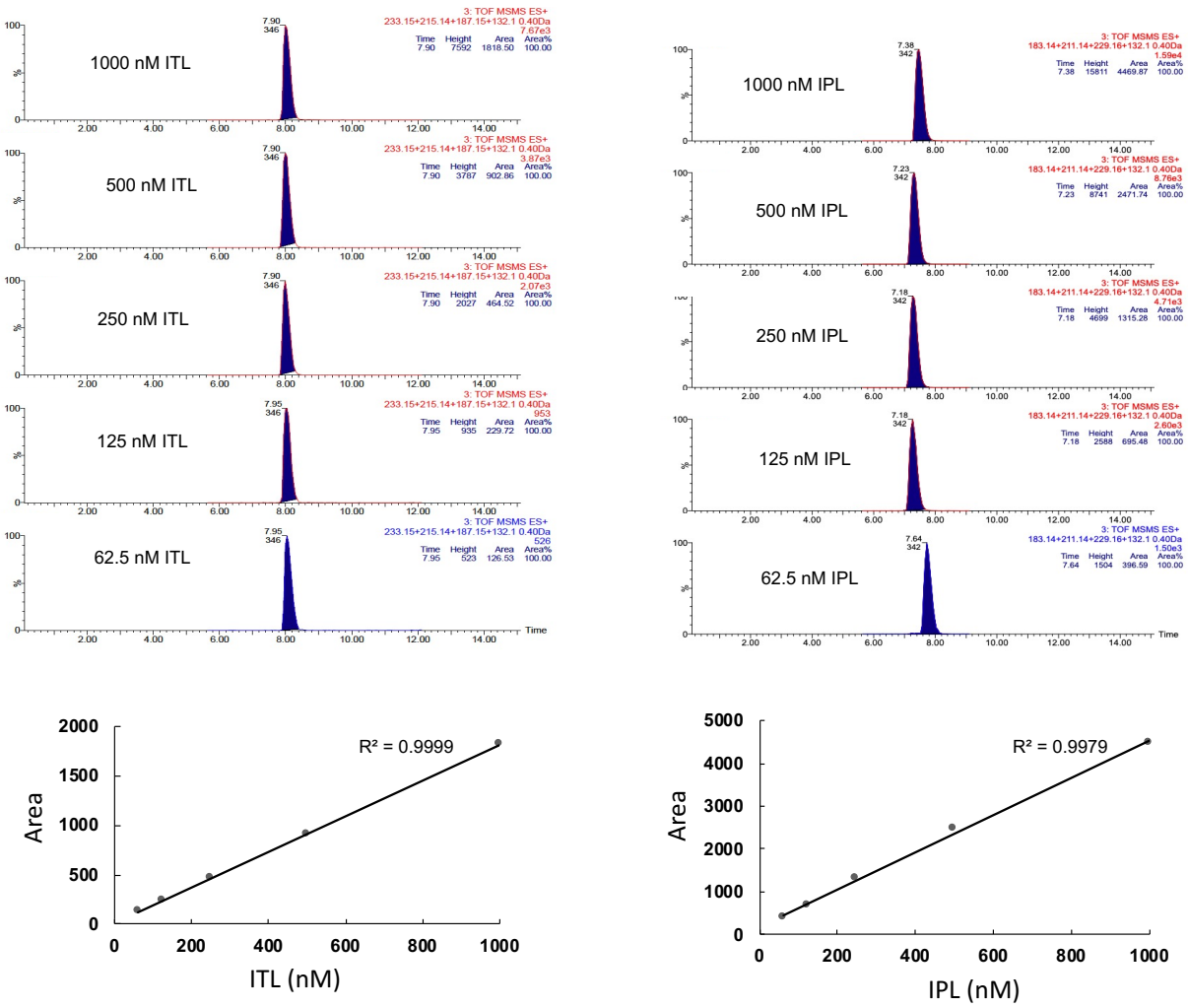

Figure S1: LC-MS/MS of all small-peptide standards (ITL and IPL) predicted to be generated for C100 substrates tested after γ-secretase digestion of substrates. Chromatograms are selected ion plots of the three most abundant sequence-specific product ions, selected with a 0.03 unit window. Standard curves for all small peptides were generated by plotting of the resulting peak areas of ion plots against the small-peptide concentration.

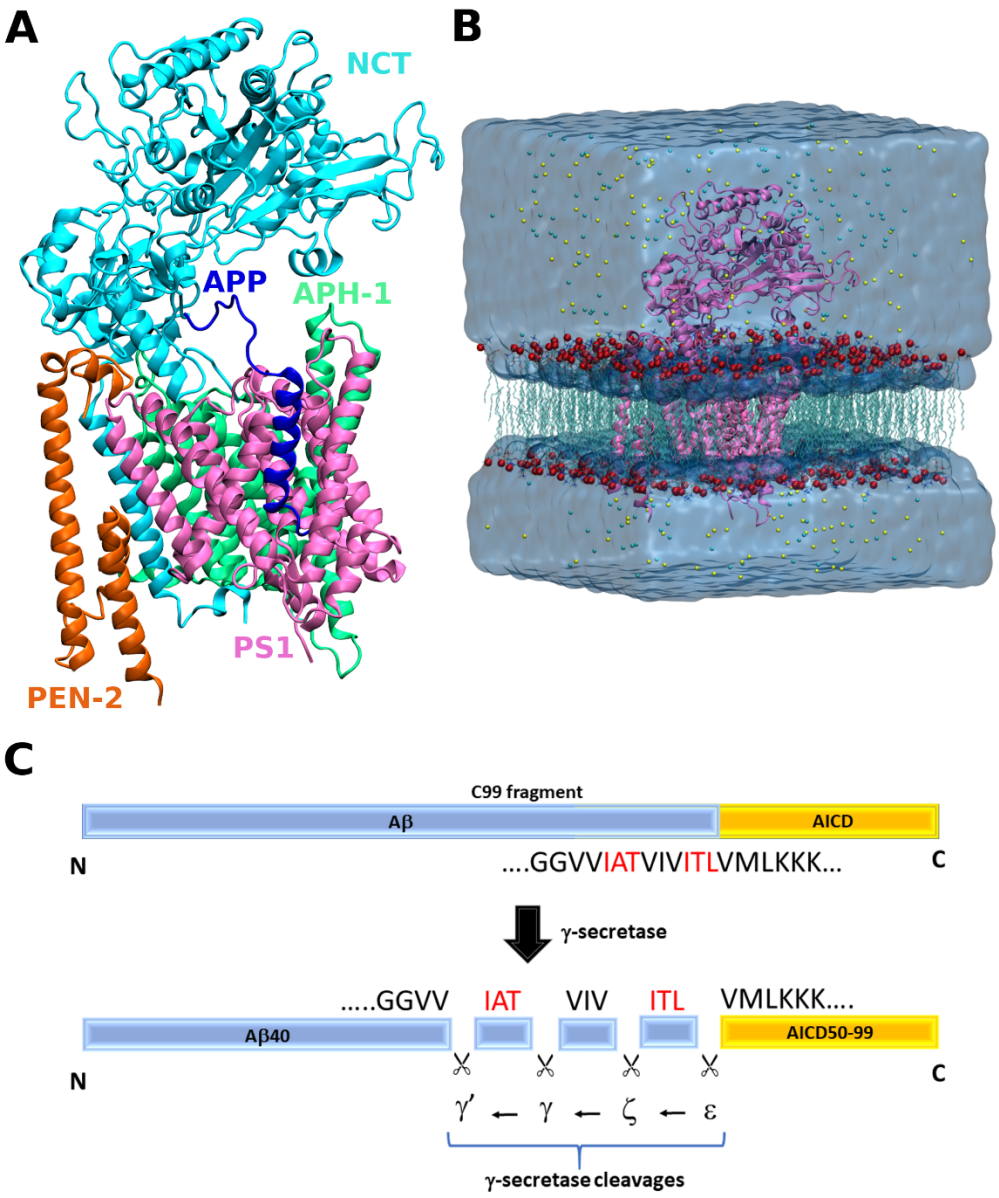

Figure S2: (A) γ-secretase structure bound to Aβ49 substrate (blue) with Niscastrin (NCT, cyan), Presenilin-1 (PS1, pink), Anterior Pharynx-Defective 1 (APH-1, green) and Presenilin Enhancer-2 (PEN-2, orange) subunits. The enzyme-substrate complex is represented in ribbons. (B) Pep-GaMD computational model of γ-secretase complex. The protein was embedded into a POPC lipid bilayer and solvated in an aqueous medium of 0.15 M NaCl. (C) Schematic representation of ε cleavage and processive proteolysis of APP substrate by γ-secretase.

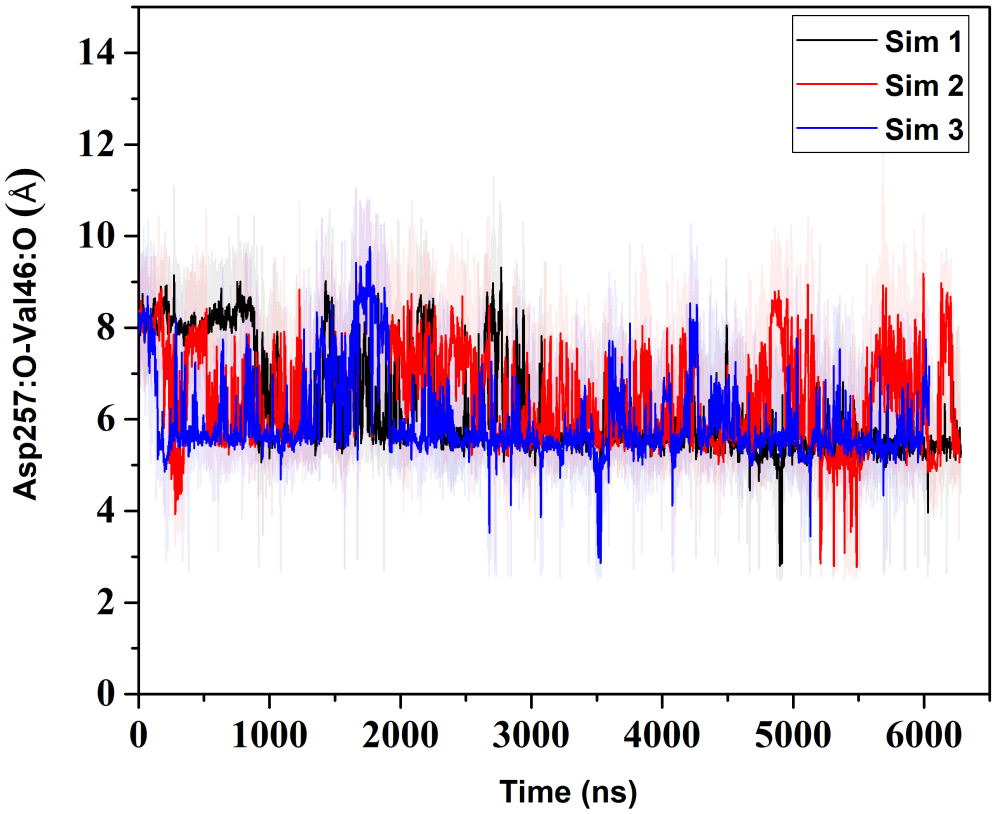

Figure S3: Timecourse of the Asp257:protonated O - Val46:O distance calculated from GaMD simulations of WT γ-secretase system. More than 6 μs long GaMD simulations of the enzyme could not capture stable activation for ζ cleavage.

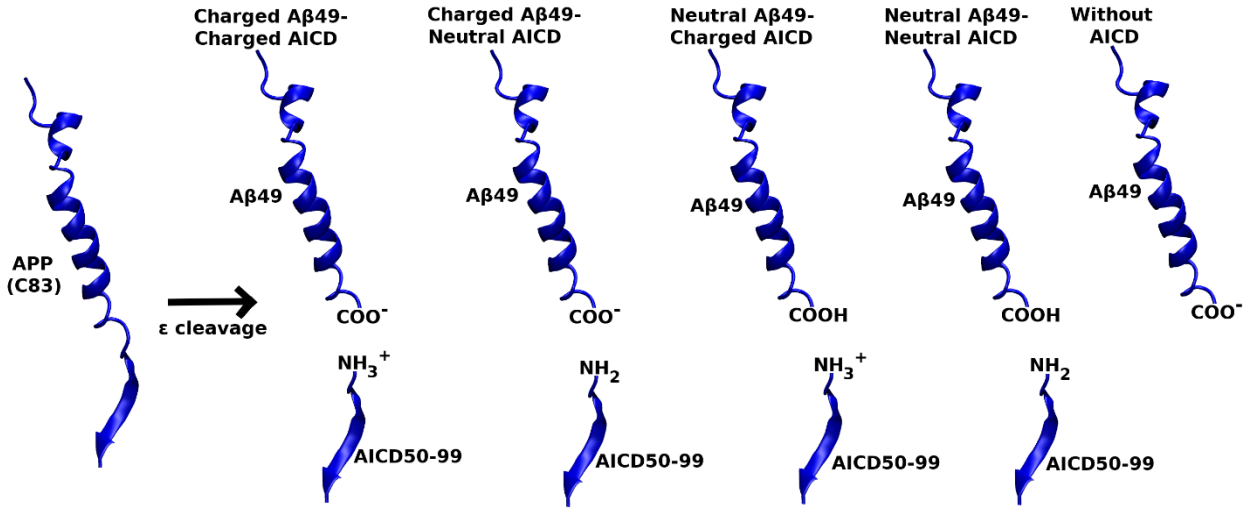

Figure S4: Ribbon representation of Aβ49 peptide and differently charged N-terminal AICD50-99 after ε cleavage of APP substrate by γ-secretase. Five different systems of γ-secretase bound to neutral and charged C-terminal Aβ49 in the absence and presence of neutral and charged N-terminal AICD were used for Pep-GaMD simulations.

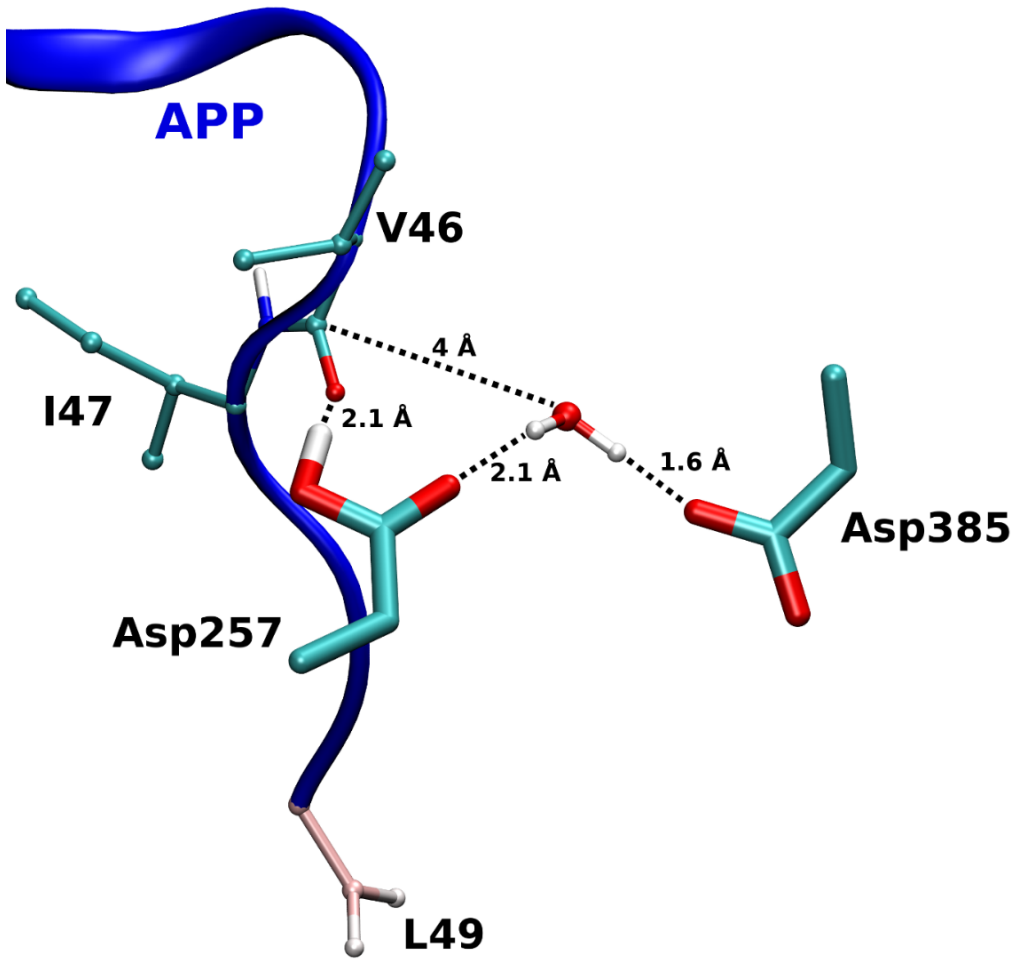

Figure S5: The active site poised for ζ cleavage proteolysis. The enzyme activation for ζ cleavage was characterized by coordinated hydrogen bonding between the enzyme Asp257 and carbonyl oxygen of C99 Val46. The water molecule could form hydrogen bond interactions with both catalytic aspartates and is at ~4 Å distance away from the carbonyl carbon of Val46 residue. The APP substrate (blue), aspartates and APP residues are shown as ribbon, stick and, balls and sticks, respectively.

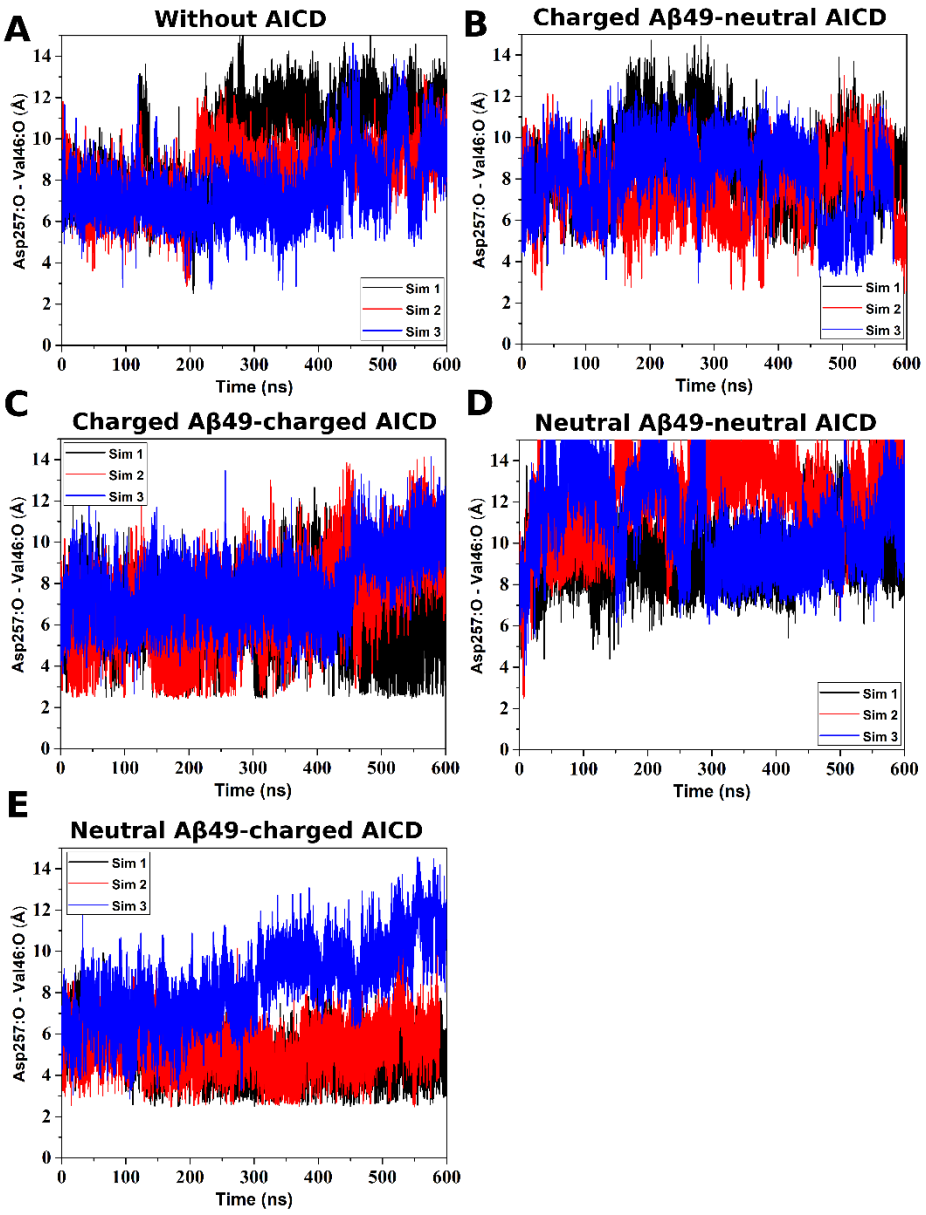

Figure S6: Time courses of the Asp257:protonated O – Val46:O distances calculated from Pep-GaMD simulations of (A) WT without AICD , (B) WT with charged Aβ49 and neutral AICD, (C) WT with charged Aβ49 and charged AICD, (D) WT with neutral Aβ49 and neutral AICD, and (E) with neutral Aβ49 and charged AICD bound γ-secretase systems.

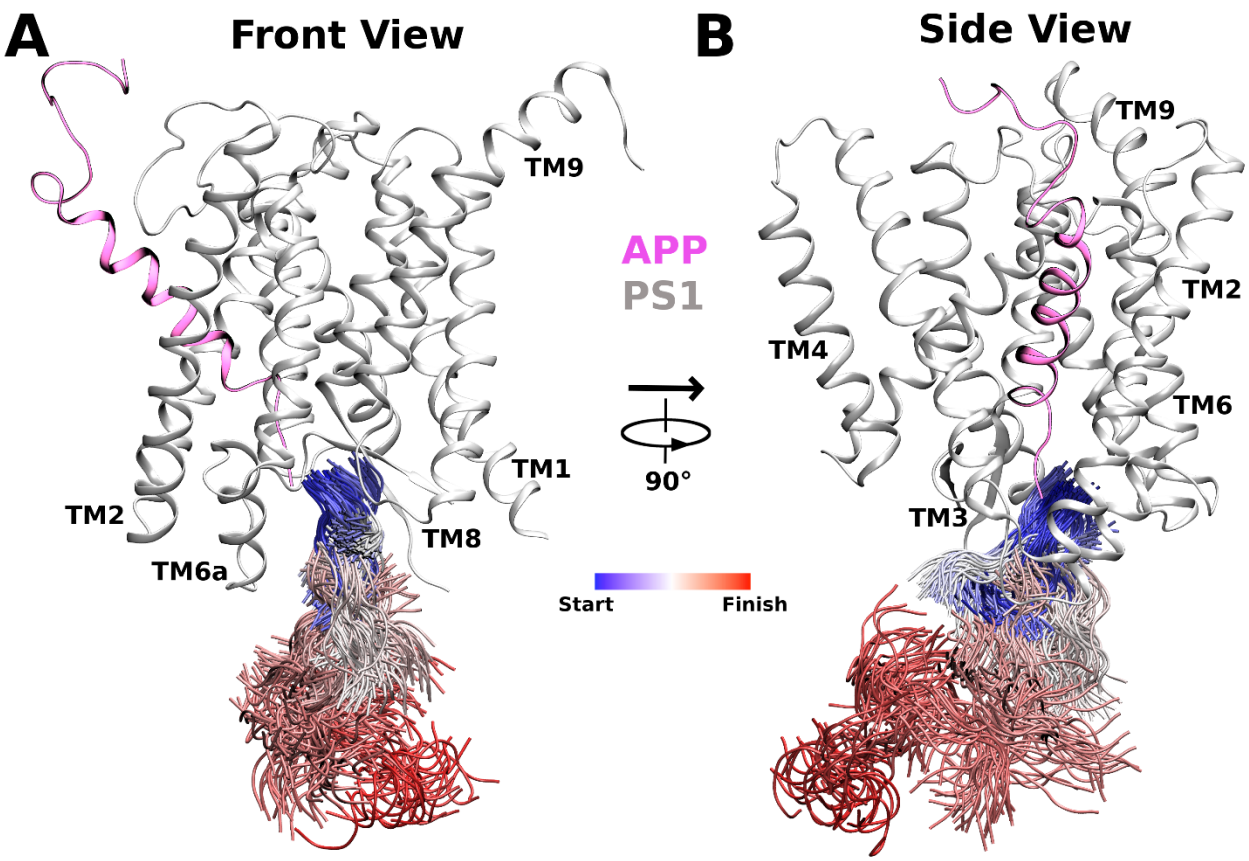

Figure S7: AICD50-99 dissociation pathway observed in Pep-GaMD simulations of γ-secretase system bound to wildtype APP colored by simulations time in a blue-white-red (BWR) color scheme.

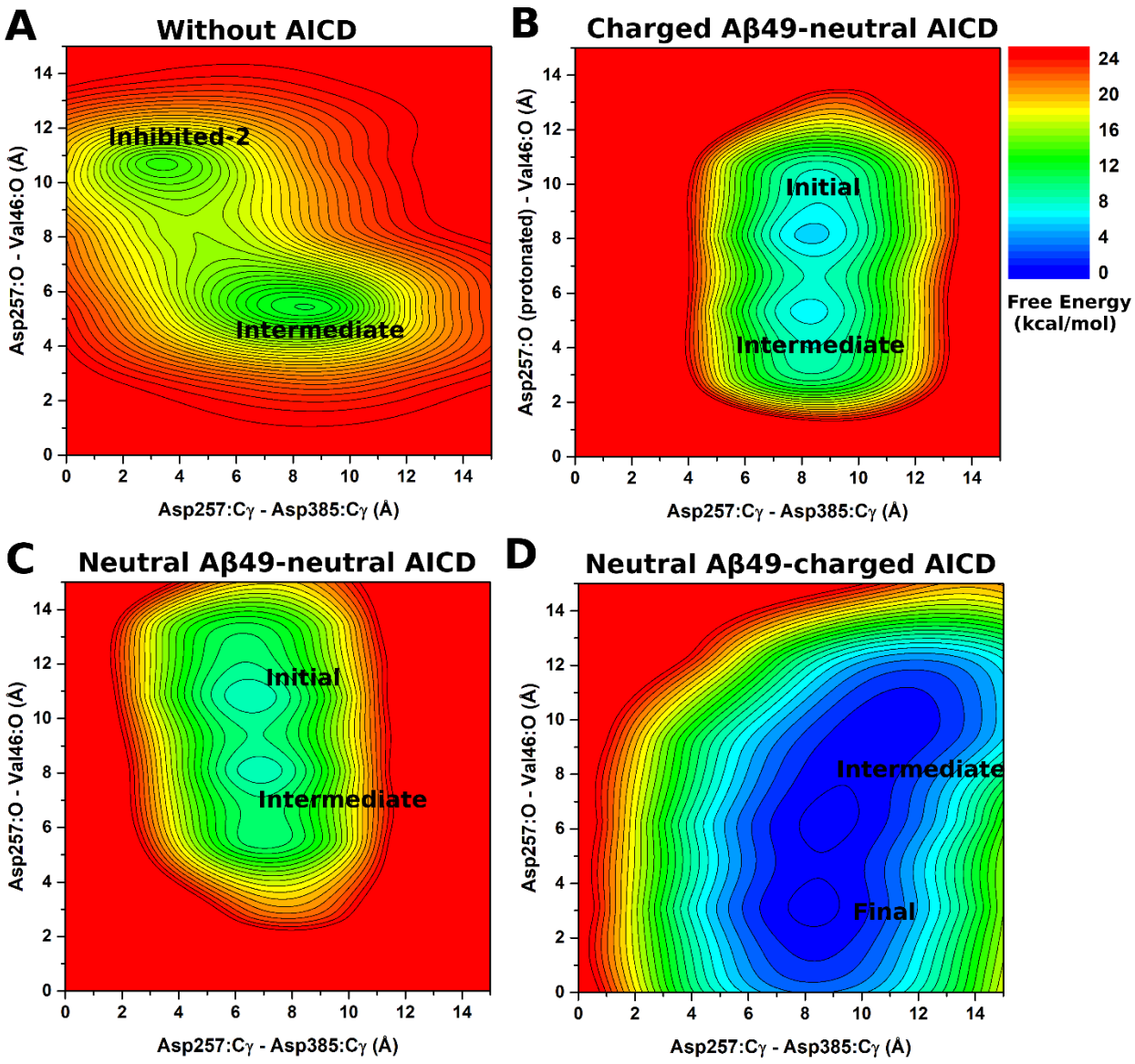

Figure S8: 2D free energy profiles of the Asp257:Cγ - Asp385:Cγ and Asp257:protonated O - Leu49:O distances calculated from Pep-GaMD simulations of (A) wildtype without AICD, (B) wildtype with charged C-terminal Aβ49 and neutral N-terminal AICD50-99, (C) wildtype with neutral C-terminal Aβ49 and neutral N-terminal AICD50-99, and (D) wildtype with neutral C-terminal Aβ49 and charged N-terminal AICD50-99 γ-secretase systems.

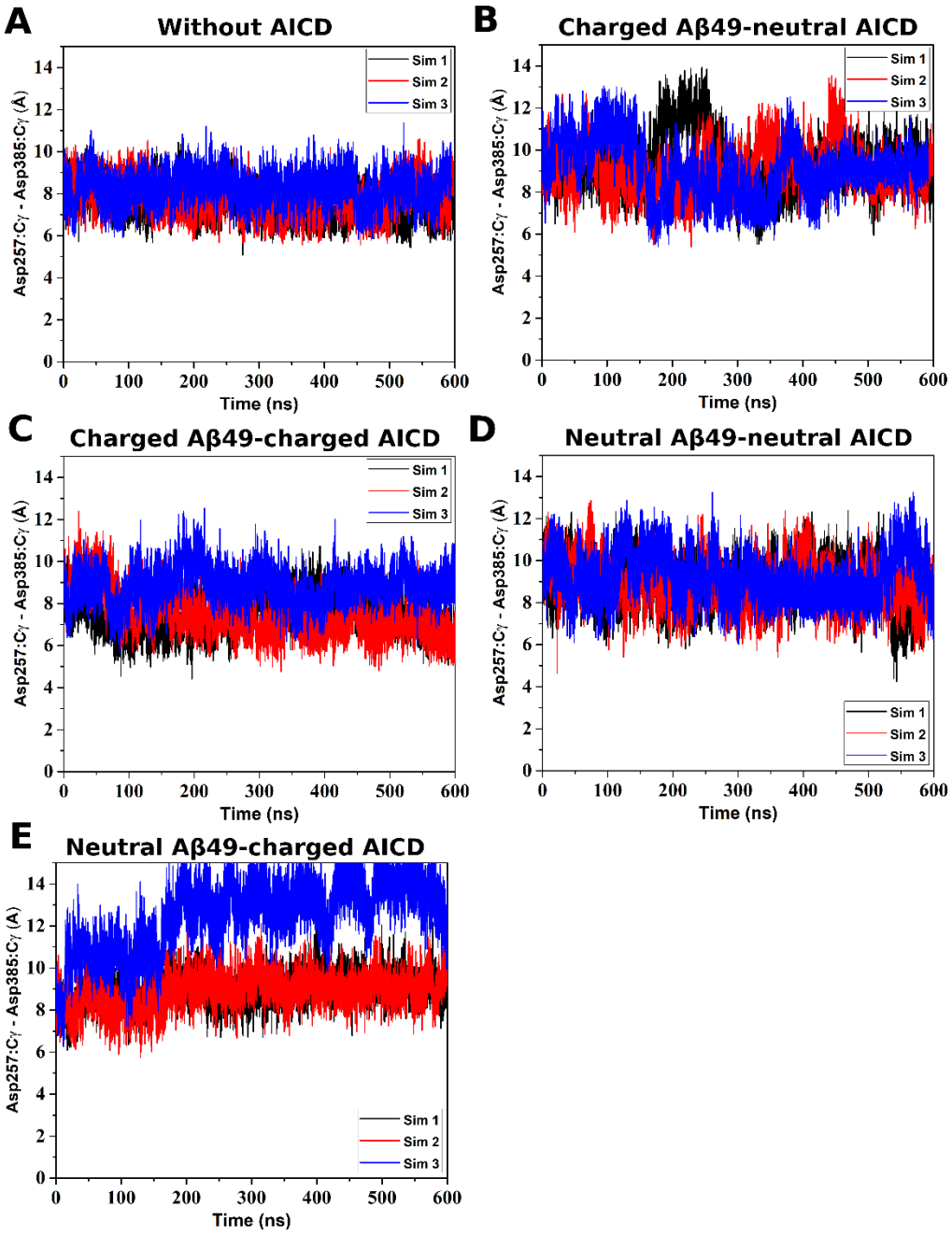

Figure S9: Time courses of the Asp257:Cγ - Asp385:Cγ distances calculated from Pep-GaMD simulations of (A) WT without AICD, (B) WT with charged Aβ49 and neutral AICD, (C) WT with charged Aβ49 and charged AICD, (D) WT with neutral Aβ49 and neutral AICD, and (E) with neutral Aβ49 and charged AICD bound γ-secretase systems.

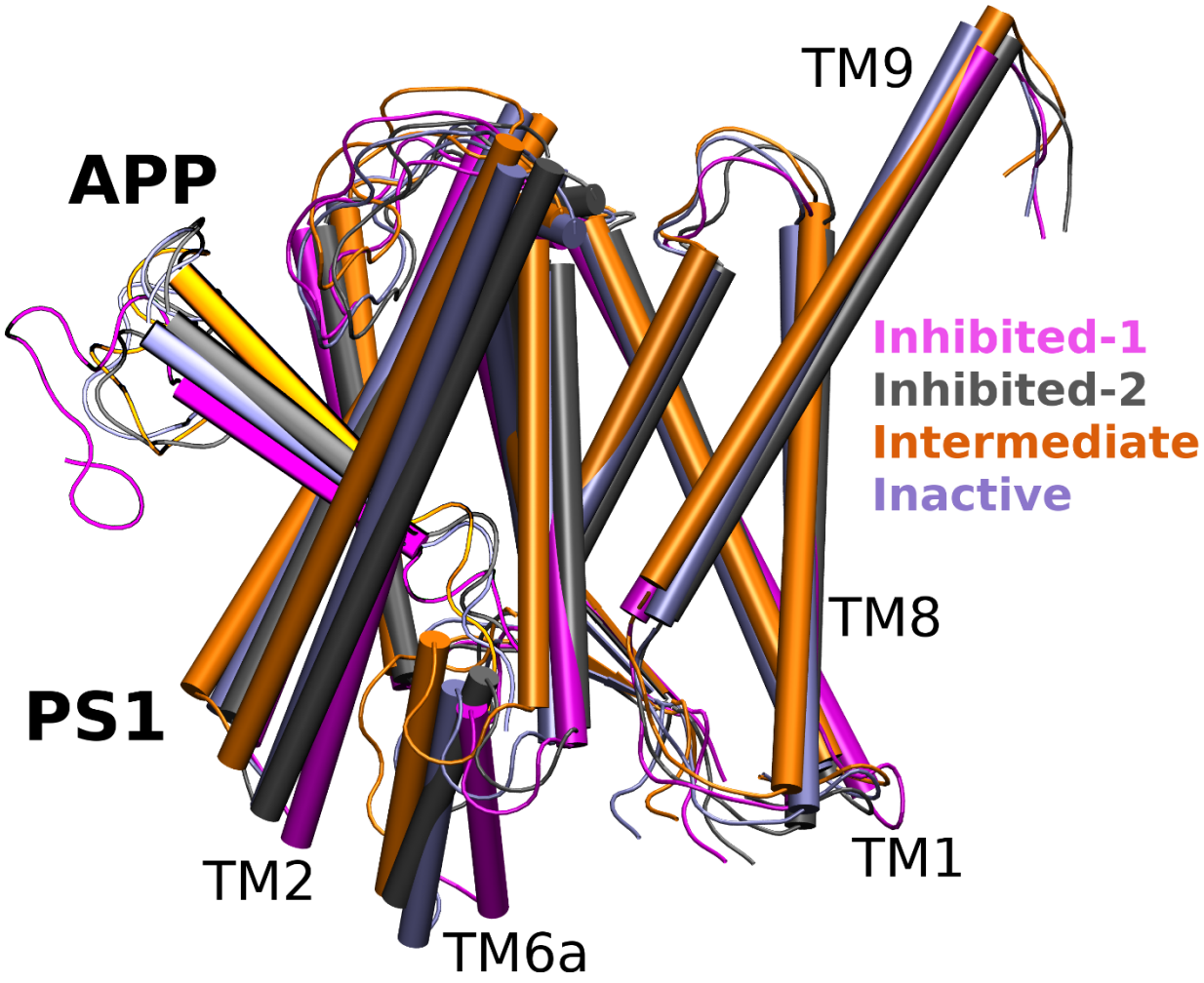

Figure S10: Comparison of different low energy state conformations as identified from Pep-GaMD free energy profiles of wildtype and mutant APP bound γ-secretase systems including Inhibited-1 (magenta), Inhibited-2 (gray), Intermediate (orange) and Inactive (ice blue) states.

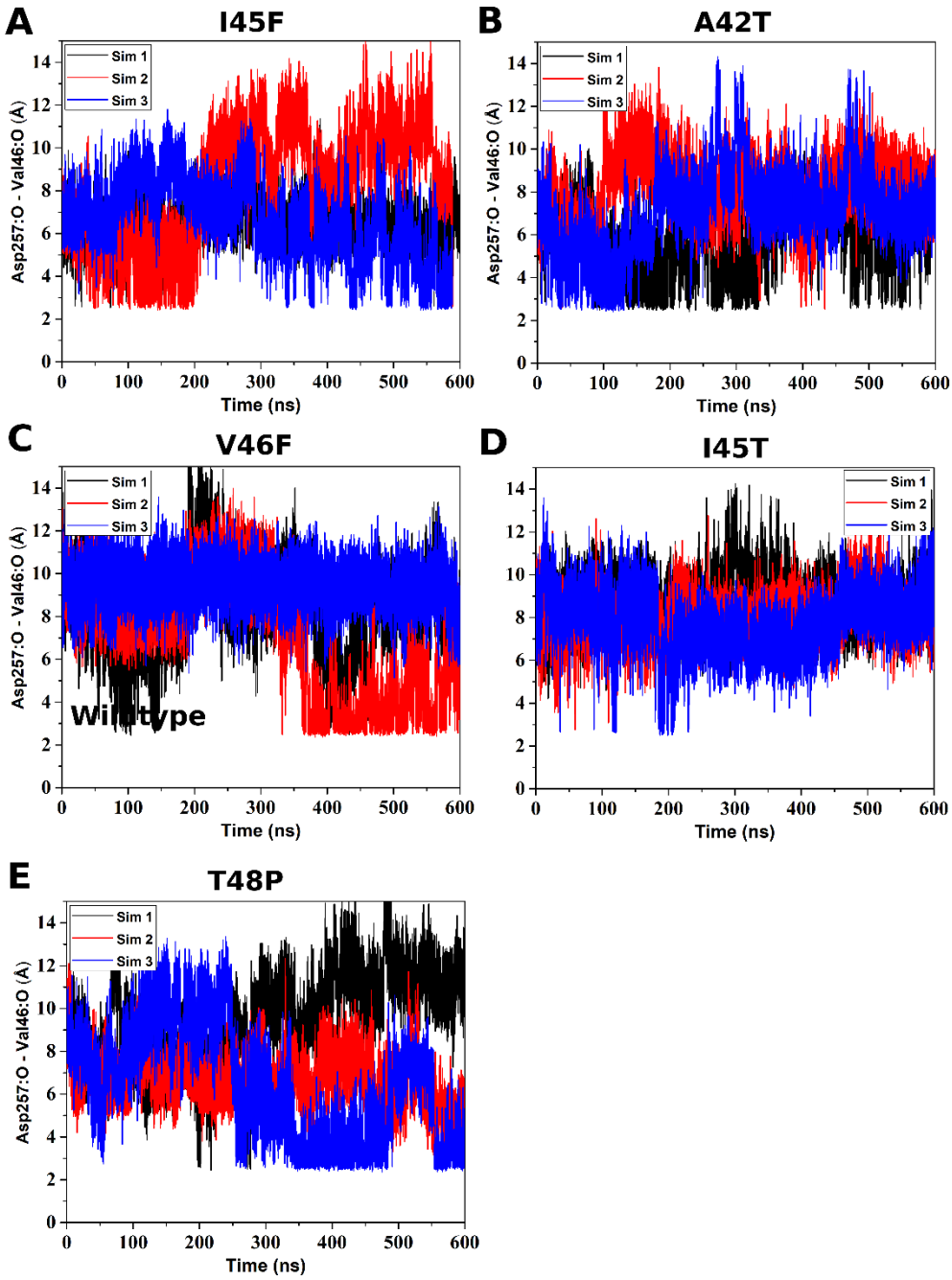

Figure S11: Time courses of the Asp257:protonated O – Val46:O distances calculated from Pep-GaMD simulations of (A) I45F, (B) A42T, (C) V46F, (D) I45T and (E) T48P APP, all with C-terminally charged Aβ49 in presence of N-terminally charged AICD, bound γ-secretase systems.

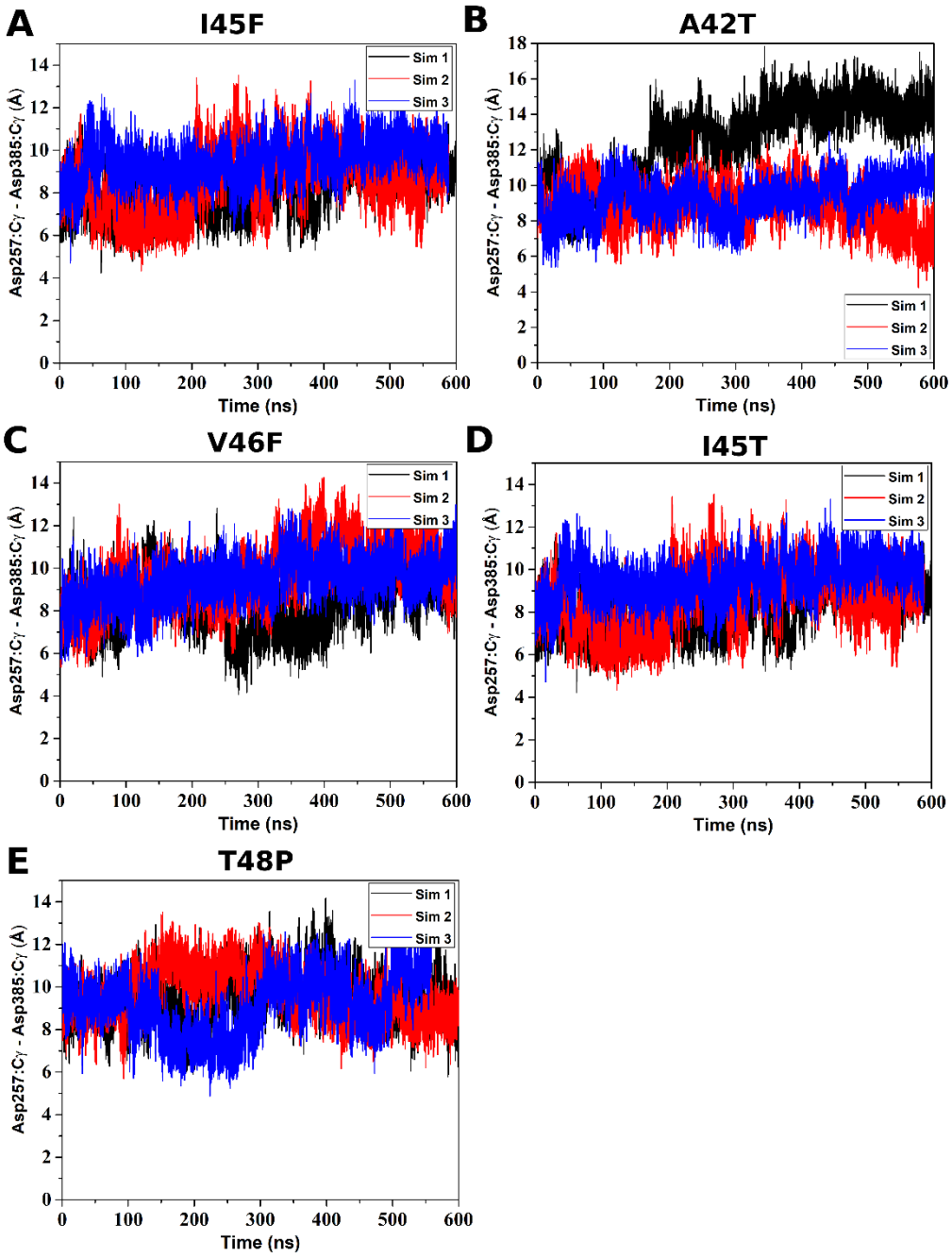

Figure S12: Time courses of the Asp257:Cγ - Asp385:Cγ distances calculated from Pep-GaMD simulations of (A) I45F, (B) A42T, (C) V46F, (D) I45T and (E) T48P APP, all with C-terminally charged Aβ49 in presence of N-terminally charged AICD, bound γ-secretase systems.

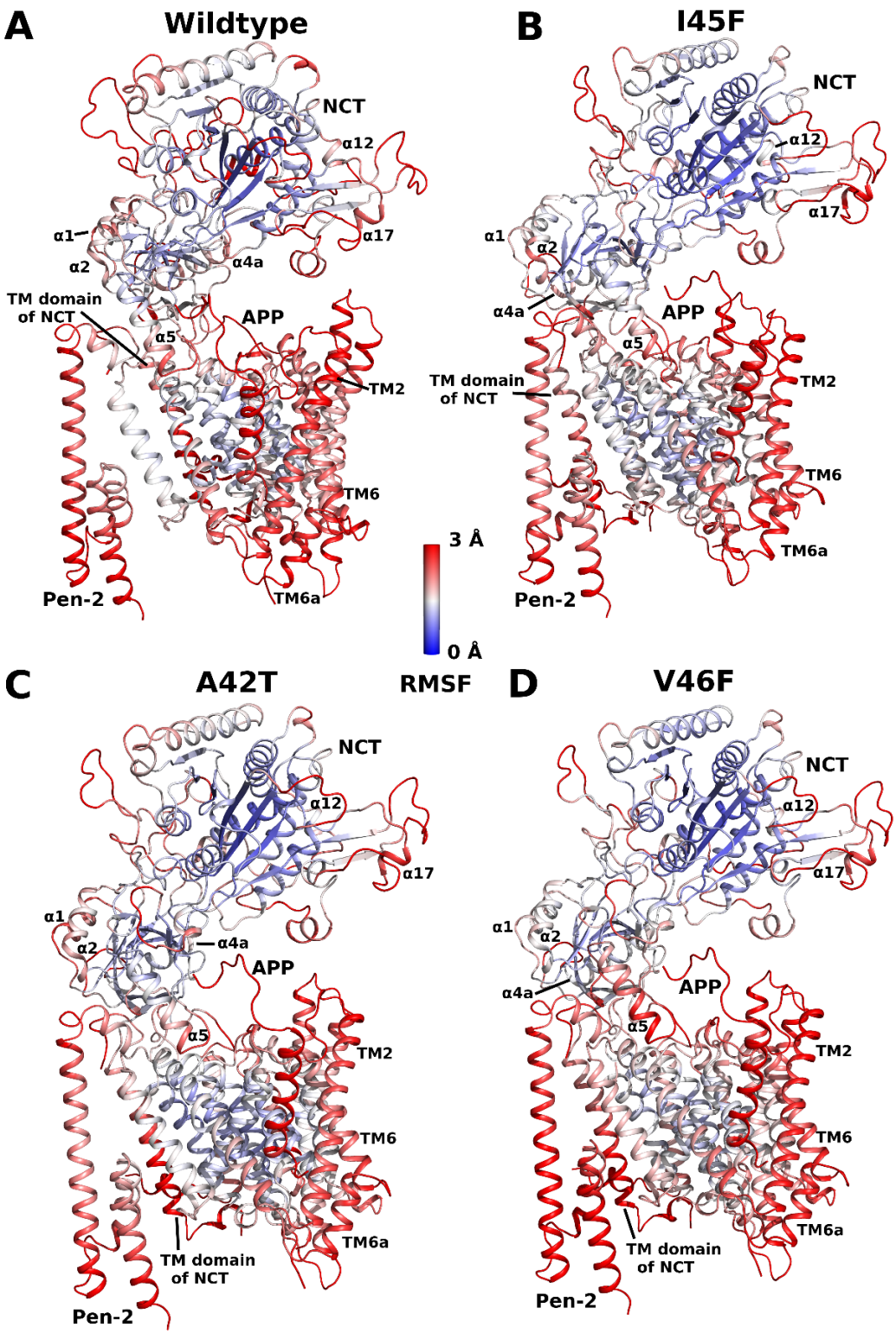

Figure S13: Root mean square fluctuation (RMSF) plots of different γ-secretase systems bound to (A) wildtype, (B) I45F mutant, (C) A42T mutant, and (D) V46F mutant APP. The RMSF is shown in blue-white-red color scheme for 0-3 Å of fluctuations in the enzyme-substrate complex.

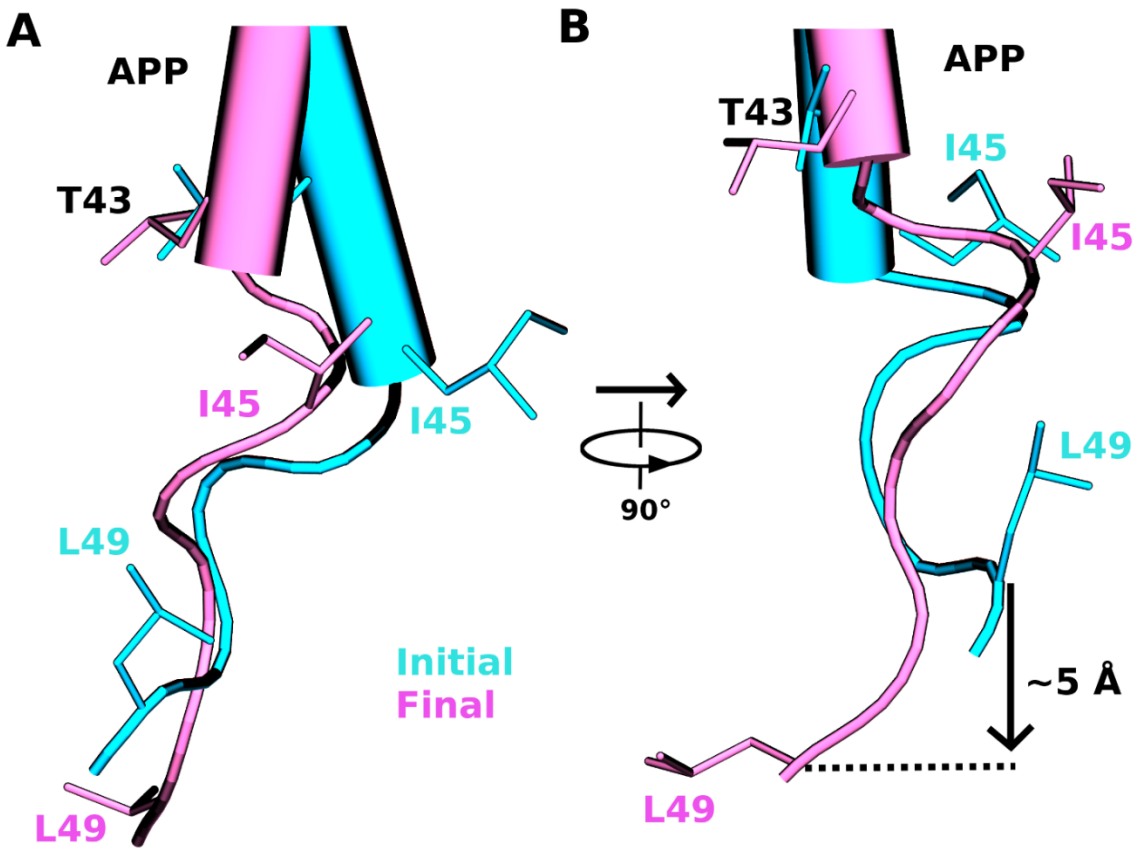

Figure S14: (A) Front and **(B)** side view comparison of relative positions of APP residues T43, I45 and L49 in the Initial and Final active states of the γ-secretase.

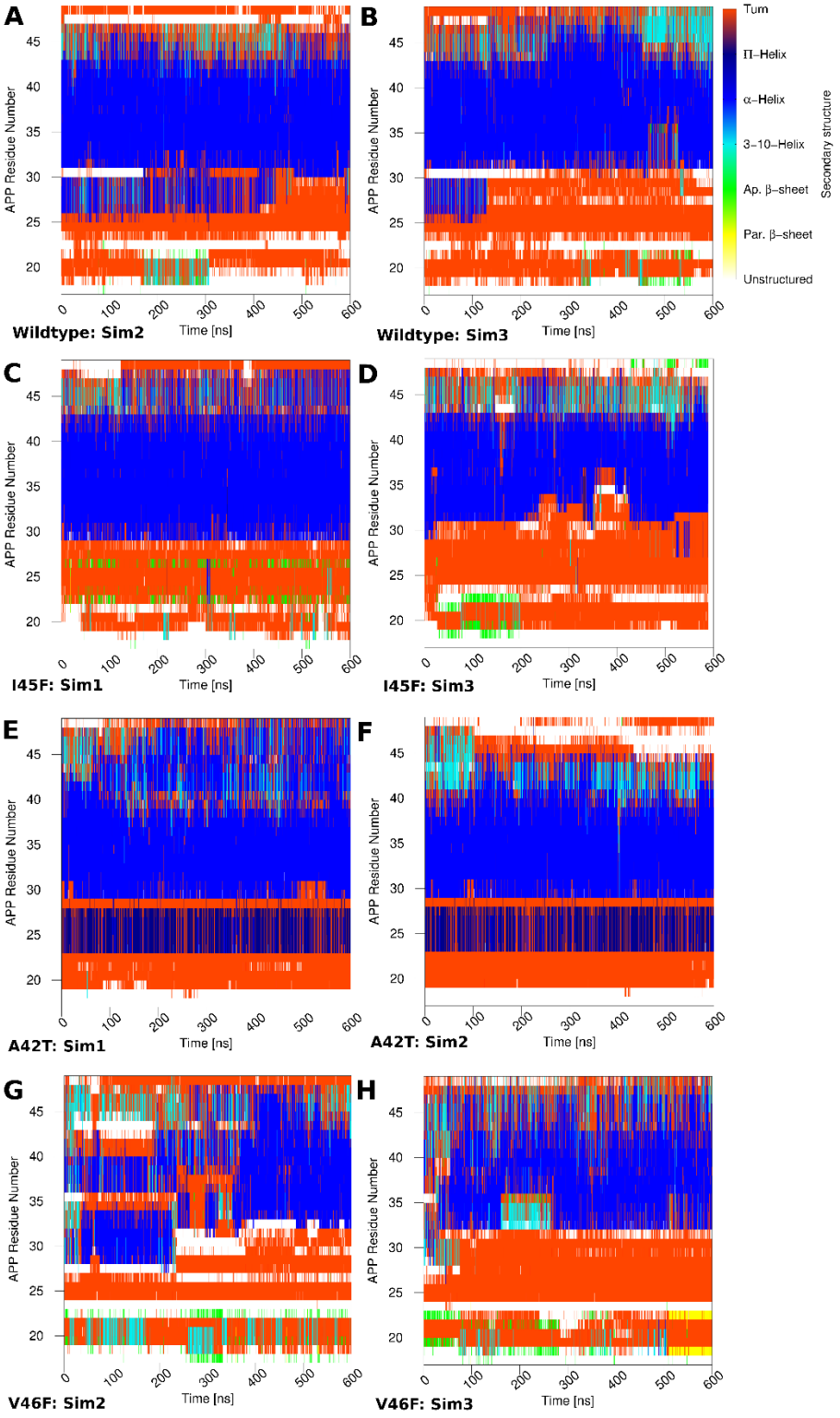

Figure S15: Time courses of secondary structures changes in the (A) Sim 2 and (B) Sim3 Pep-GaMD simulations of WT, (C) Sim 1 and (D) Sim 3 Pep-GaMD simulations of I45F, (E) Sim1 and (F) Sim2 Pep-GaMD simulations of A42T, (G) Sim2 and (H) Sim3 Pep-GaMD simulations of V46F mutant APP bound to γ-secretase.

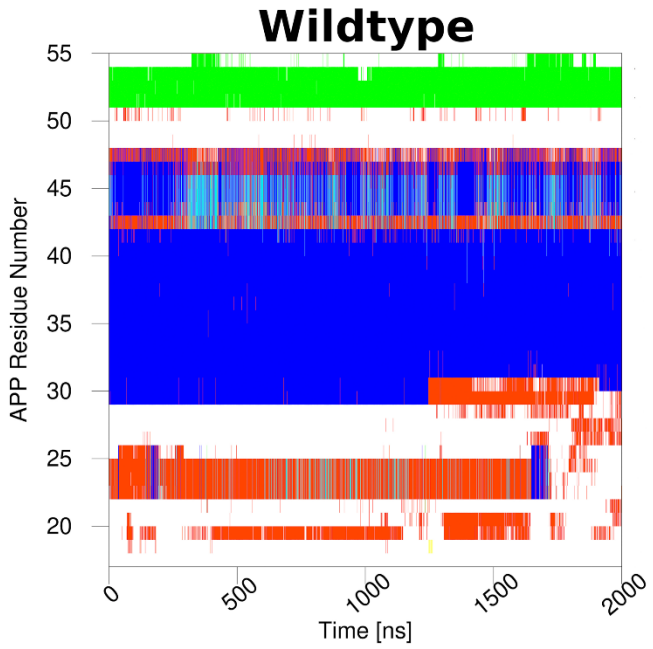

Figure S16: Time course of secondary structure changes in the GaMD simulations of WT APP substrate-bound γ-secretase recorded during enzyme activation for e cleavage. This plot is extracted from our previous study (Bhattarai, Apurba, et al. *ACS central science* 6.6 (2020): 969-983.).

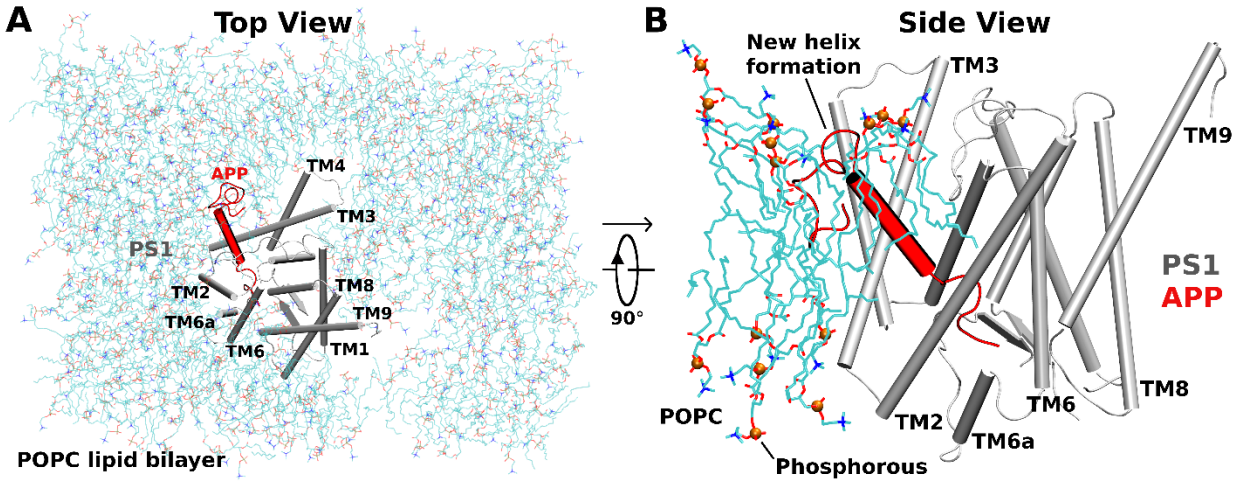

Figure S17: (A) Top and (B) Side view of APP (Aβ49) bound γ-secretase PS1 interacting with the POPC lipid bilayer membrane. The N-terminus of APP substrate during the ζ cleavage activation bends and interacts with the hydrophobic lipid bilayer to form α-helix conformation.

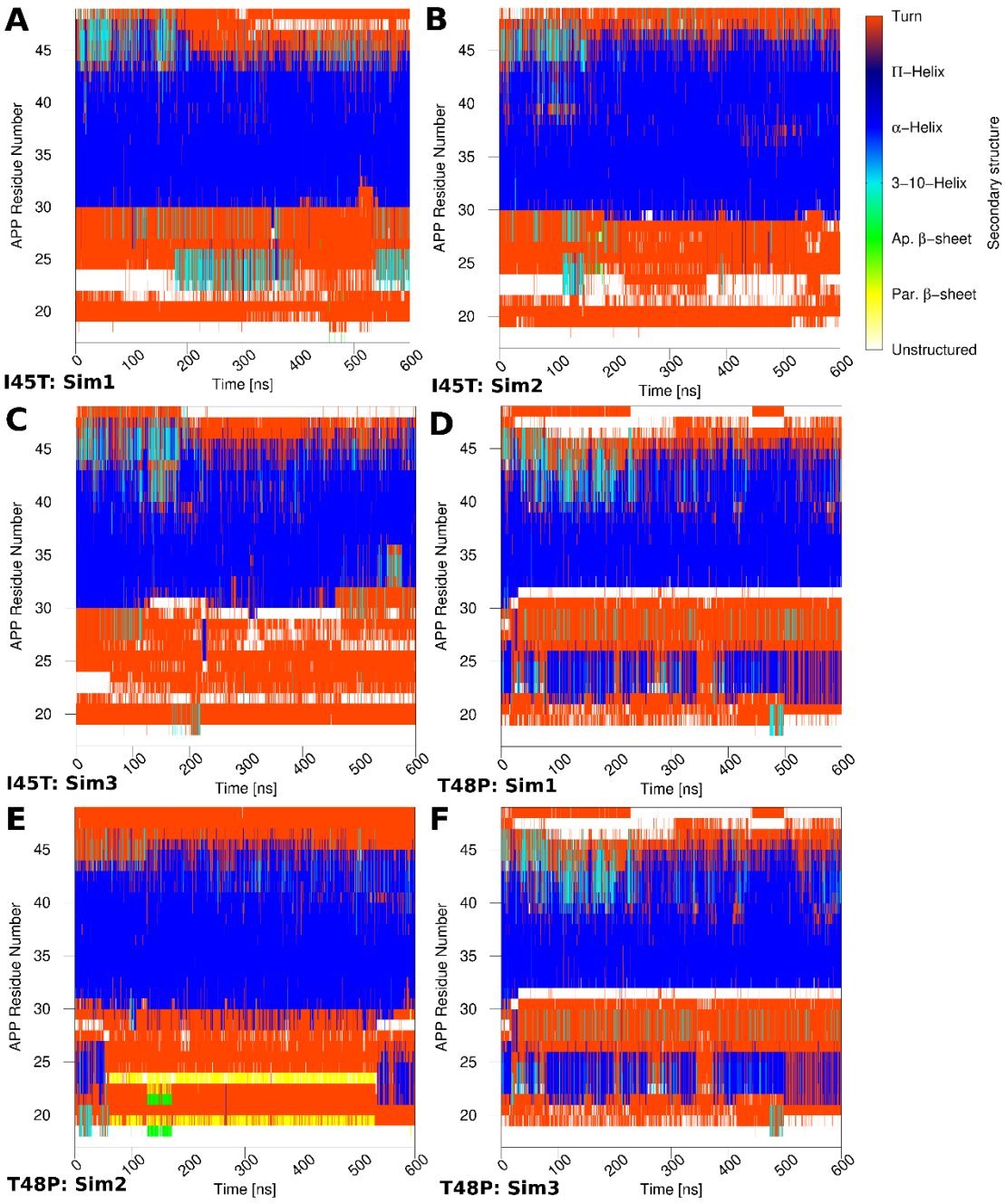

Figure S18: Time courses of secondary structure changes in the (A) Sim 1, (B) Sim2 and (C) Sim3 Pep-GaMD simulations of I45T mutant and (D) Sim 1, (E) Sim2 and (F) Sim3 Pep-GaMD simulations of T48P mutant APP bound to γ-secretase.

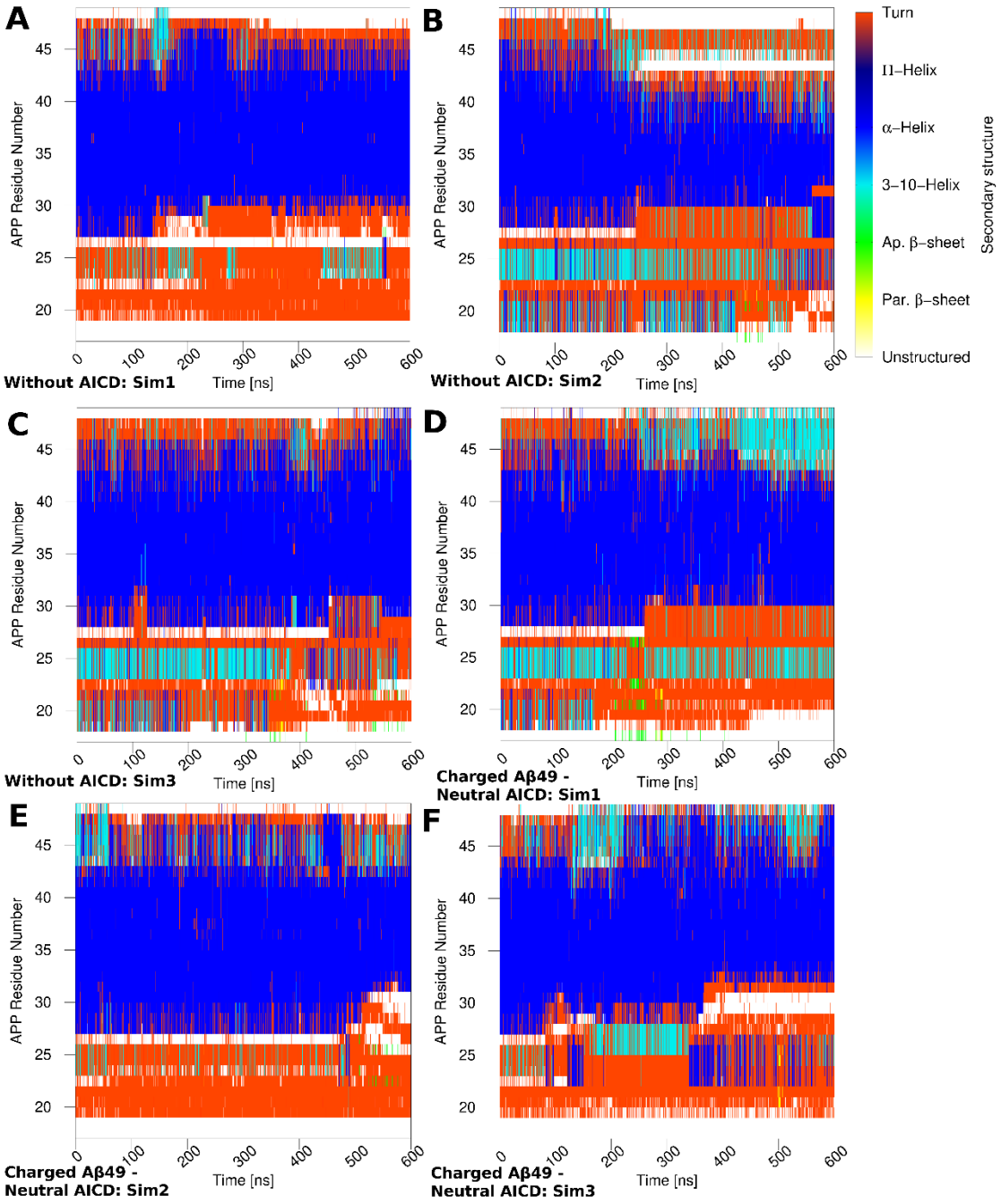

Figure S19: Time courses of secondary structure changes in the (A) Sim 1, (B) Sim2 and (C) Sim3 Pep-GaMD simulations of wildtype without AICD and (D) Sim 1, (E) Sim2 and (F) Sim3 Pep-GaMD simulations of wildtype with neutral AICD bound to γ-secretase.

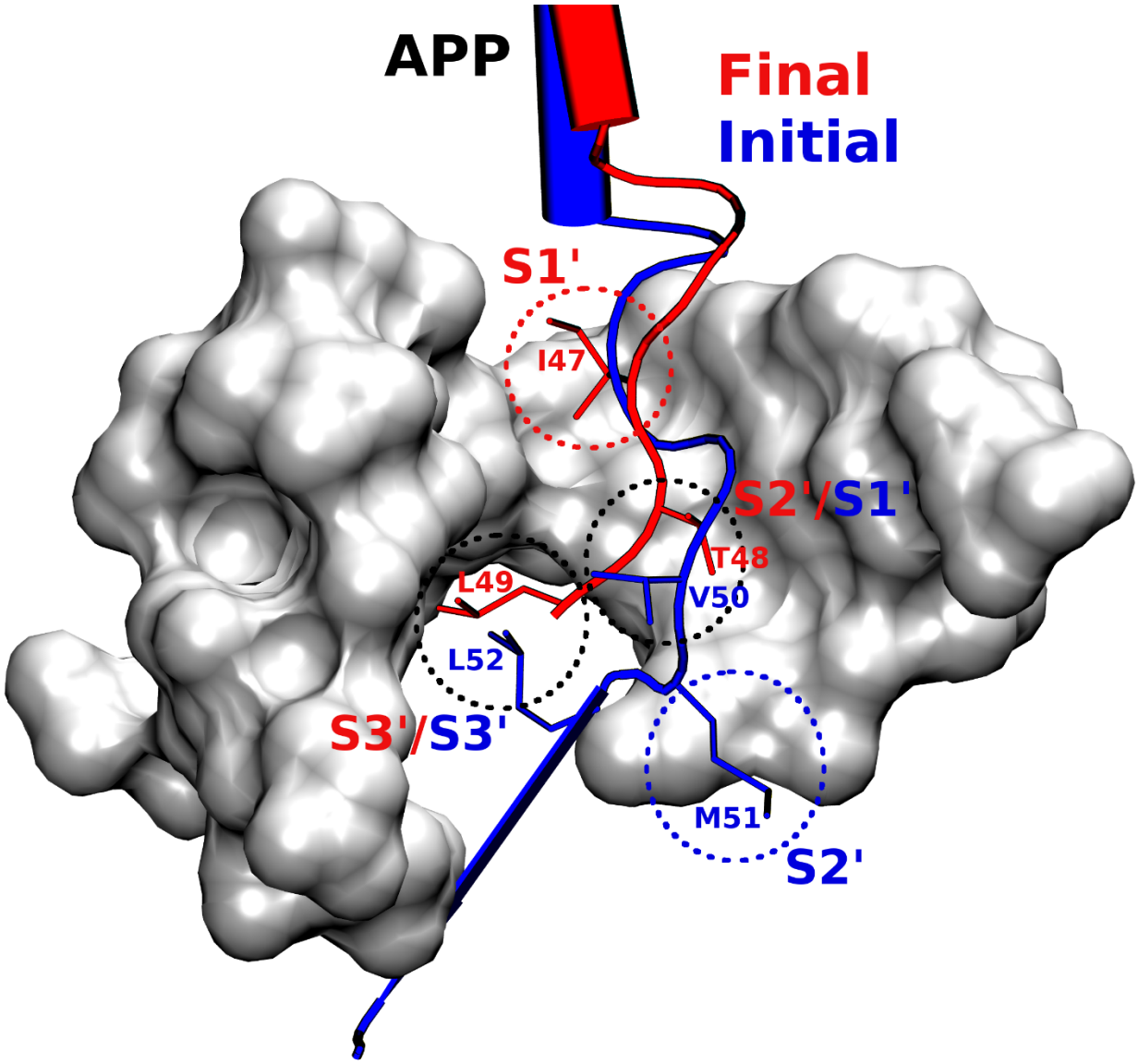

Figure S20: Comparison of active site subpockets of the Final active state during ζ cleavage to that of the Initial active state during ε cleavage.

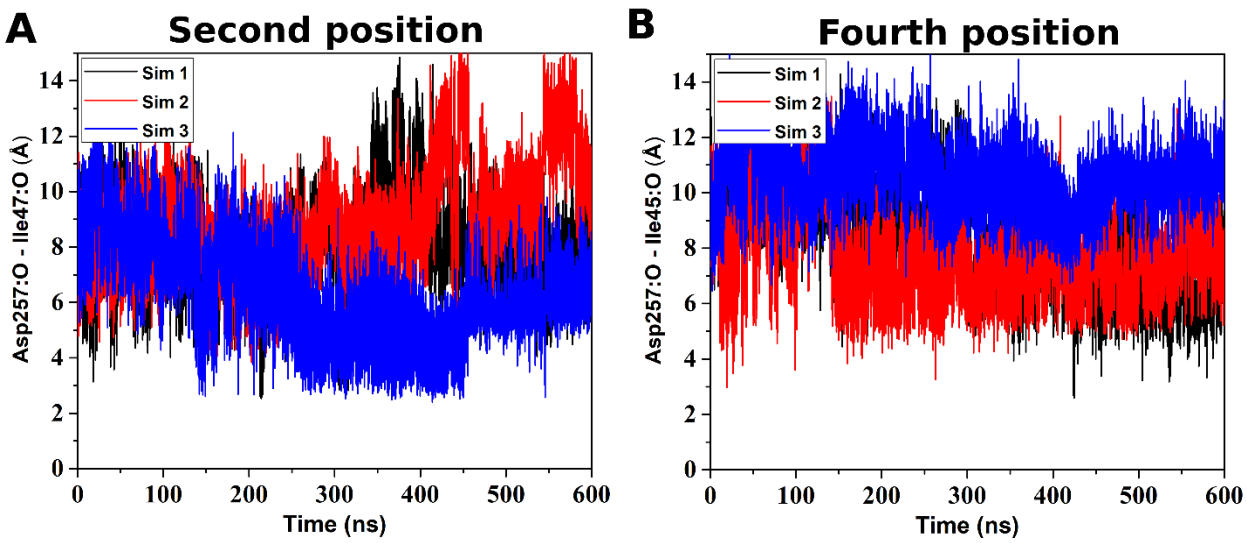

Figure S21: Time courses of the (A) Asp257:protonated O – Ile47:O and (B) Asp257:protonated O – Ile45:O distances calculated from Pep-GaMD simulations of WT with charged Aβ49 and charged AICD bound γ-secretase systems representing two and four amino acid residues shift for cleavage starting from activated enzyme for ε cleavage, respectively.

Table S1: Residues constituting the active site subpockets S1', S2' and S3' occupied by P1', P2' and P3' Aβ49 residues for different γ-secretase systems bound to wildtype and I45F, A42T and V46F FAD mutant Aβ49.

System	S1'	S2'	S3'
Wildtype/I45F/A42T	L249 Y256 L268 I287 L286 L271 L272 L150 T147 L282 F283 W165 V261 G382 L383 G384	P433 L435 L258 V261 L268 K380 L381 G382	L268 L271 V272 A275 L282 F283 I287 L381 G382 L383 I287
V46F	I253 T147 Y256 L268 L271 M146	L249 Y256 L268 I287 L286 L271 L272 L150 T147 L282 F283 W165 V261 G382 L383 G384	L268 L271 V272 A275 L282 F283 I287 L381 G382 L383 I287

Table S2: Summary of Pep-GaMD simulations on five different γ-secretase systems bound to neutral/charged C-terminal Aβ49 in the absence or presence of neutral/charged N-terminal AICD50-99 peptide. "Activation" denotes that the Pep-GaMD simulations could capture activation of γ-secretase for the ζ cleavage of Aβ49, and otherwise denoted "No activation".

Aβ49 C-terminus / **AICD N-terminus**	**Neutral**	**Charged**
Neutral	No activation	No activation
Charged	Activation	Activation
Absent	-	No activation

Supporting Movies Captions

Movie S1
Activation of γ-secretase for ζ cleavage of Aβ49 was captured in Pep-GaMD simulations (Sim1 in Fig. S6C). The enzyme activation for ζ cleavage was characterized by coordinated hydrogen bonding between the enzyme Asp257 and carbonyl oxygen of substrate Val46. The catalytic aspartates were at a distance of ~7-8 Å between their Cγ atoms, which could accommodate a water molecule for nucleophilic attack of the carbonyl carbon of the scissile amide bond.

Movie S2
The AICD50-99 fragment dissociated from PS1 to the intracellular bulk solvent during activation of γ-secretase for ζ cleavage of Aβ49 in Pep-GaMD simulations.

Movie S3
Activation of γ-secretase for ζ cleavage of I45F FAD mutant Aβ49 was captured in Pep-GaMD simulations (Sim2 in Fig. S6D). The enzyme activation for ζ cleavage was characterized by coordinated hydrogen bonding between the enzyme Asp257 and carbonyl oxygen of substrate Val46.

Movie S4
Activation of γ-secretase for ζ cleavage of A42T FAD mutant Aβ49 was captured in Pep-GaMD simulations (Sim3 in Fig. S6E). The enzyme activation for ζ cleavage was characterized by coordinated hydrogen bonding between the enzyme Asp257 and carbonyl oxygen of substrate Val46.

Movie S5
Activation of γ-secretase for ζ cleavage of V46F FAD mutant Aβ49 was captured in Pep-GaMD simulations (Sim1 in Fig. S6F). The enzyme activation for ζ cleavage was characterized by coordinated hydrogen bonding between the enzyme Asp257 and carbonyl oxygen of substrate Phe46.

Movie S6
Fluctuations of catalytic domain PS1 and substrate Aβ49 during the activation of γ-secretase for ζ cleavage in Pep-GaMD simulations (Sim1 in Fig. S6C).

References

1. Li, Y.-M.; Lai, M.-T.; Xu, M.; Huang, Q.; DiMuzio-Mower, J.; Sardana, M. K.; Shi, X.-P.; Yin, K.-C.; Shafer, J. A.; Gardell, S. J., Presenilin 1 is linked with γ-secretase activity in the detergent solubilized state. *Proceedings of the National Academy of Sciences* **2000,** *97* (11), 6138-6143.
2. Bhattarai, A.; Devkota, S.; Bhattarai, S.; Wolfe, M. S.; Miao, Y., Mechanisms of γ-Secretase Activation and Substrate Processing. *ACS Central Science* **2020**.
3. Devkota, S.; Williams, T. D.; Wolfe, M. S., Familial Alzheimer's disease mutations in amyloid protein precursor alter proteolysis by γ-secretase to increase amyloid β-peptides of≥ 45 residues. *Journal of Biological Chemistry* **2021,** *296*, 100281.
4. Wang, J.; Miao, Y., Peptide Gaussian accelerated molecular dynamics (Pep-GaMD): Enhanced sampling and free energy and kinetics calculations of peptide binding. *The Journal of Chemical Physics* **2020,** *153* (15), 154109.
5. Zhou, R.; Yang, G.; Guo, X.; Zhou, Q.; Lei, J.; Shi, Y., Recognition of the amyloid precursor protein by human γ-secretase. *Science* **2019,** *363* (6428).
6. Waterhouse, A.; Bertoni, M.; Bienert, S.; Studer, G.; Tauriello, G.; Gumienny, R.; Heer, F. T.; de Beer, T. A. P.; Rempfer, C.; Bordoli, L., SWISS-MODEL: homology modelling of protein structures and complexes. *Nucleic acids research* **2018,** *46* (W1), W296-W303.
7. Case, D. A.; Belfon, K.; Ben-Shalom, I.; Brozell, S. R.; Cerutti, D.; Cheatham, T.; Cruzeiro, V. W. D.; Darden, T.; Duke, R. E.; Giambasu, G., Amber 2020. **2020**.
8. Pang, Y. T.; Miao, Y.; Wang, Y.; McCammon, J. A., Gaussian Accelerated Molecular Dynamics in NAMD. *J Chem Theory Comput* **2017,** *13* (1), 9-19.
9. Miao, Y.; Feher, V. A.; McCammon, J. A., Gaussian Accelerated Molecular Dynamics: Unconstrained Enhanced Sampling and Free Energy Calculation. *Journal of Chemical Theory and Computation* **2015,** *11* (8), 3584-3595.
10. Humphrey, W.; Dalke, A.; Schulten, K., VMD: Visual molecular dynamics. *J Mol Graph Model* **1996,** *14* (1), 33-38.
11. Roe, D. R.; Cheatham, T. E., PTRAJ and CPPTRAJ: Software for Processing and Analysis of Molecular Dynamics Trajectory Data. *Journal of Chemical Theory and Computation* **2013,** *9* (7), 3084-3095.
12. Miao, Y.; Sinko, W.; Pierce, L.; Bucher, D.; McCammon, J. A., Improved reweighting of accelerated molecular dynamics simulations for free energy calculation. *Journal of Chemical Theory and Computation* **2014,** *10* (7), 2677–2689.